Influence of Organic Matter Source, Abundance, and Growth Habit on Depositional Textures and Associated Pore Attributes of Hypersaline Lacustrine Microbial Deposits (Holocene, Bahamas)

By

Hannah Lynn Hubert

Submitted to the graduate degree program in Geology and the Graduate Faculty of the University of Kansas in partial fulfillment of the requirements for the degree of Master of Science.

_____

Chair: Dr. Eugene C. Rankey

_____

Dr. Alison Olcott-Marshall

_____

Dr. Chi Zhang

Date Defended: May 17th, 2017

The Thesis Committee for Hannah Lynn Hubert
certifies that this is the approved version of the following thesis:

Influence of Organic Matter Source, Abundance, and Growth Habit on Depositional Textures and Associated Pore Attributes of Hypersaline Lacustrine Microbial Deposits (Holocene, Bahamas)

_____

Chair: Dr. Eugene C. Rankey

_____

Dr. Alison Olcott-Marshall

_____

Dr. Chi Zhang

Date approved: June 11th, 2017

Abstract

Discovery of lacustrine microbialite reservoirs in South Atlantic pre-salt has motivated the search for analogs for perspectives on their deposition and initial porosity. Although previous efforts mapped spatial patterns and produced facies models of large microbial lacustrine systems, details of the origins of microbialite fabrics are less well constrained. To address these unknowns, this study evaluates the influence of organic matter source, abundance, and growth habit on Holocene microbialite fabrics.

Integrated multi-scale analyses characterize fabrics of Holocene microbialites in a small, shallow, hypersaline, alkaline lake in the southern Bahamas. The results of analyses reveal: systematic distribution of surface sediment, unlithified microbial mats, and microbialites; microbialite fabrics vary considerably on several scales, and porosity varies from 43 to 59%; and organic matter abundance, rather than source, is interpreted to control fabric. Although ultimate preservation is unknown, understanding the genesis of primary fabrics may provide insights into pore evolution in reservoir analogs.

Acknowledgements

This research project was funded by Kansas Interdisciplinary Carbonates Consortium (KICC) at the University of Kansas, Art Saller and Jennifer Lewis of Cobalt International Energy of Houston, Texas, and the Society of Sedimentary Geology. First, I thank Dr. Gene Rankey as he provided me with considerable support and guidance during both my undergraduate and graduate programs, which led to acquiring my degree in a timely manner. He assured that I was successful both at the University of Kansas as well as in my future endeavors as both a person and geologist. I thank my committee members, Alison Olcott-Marshall and Chi Zhang, and microbiologist, Christopher Omelon, for providing me with expertise in their respective disciplines and for their aid in shaping the direction of this project. T.J. Waller and others at Anadarko Petroleum Corporation shared valuable preliminary results and Abdul Wahab collected a few samples and provided preliminary observations, so I also thank them for their contributions to this study.

Thanks to the people of Crooked Island, Bahamas, for being generous hosts during my fieldwork over the summer of 2016, especially Dennis Thompson for transporting me to and from my research area every day and helping with logistics during our time in the Bahamas. In addition, thanks to Adrienne Duarte for being an exceptionally organized and helpful field assistant. Furthermore, I thank her, along with all of my research group members for their assistance and advice throughout my years at the University of Kansas.

Finally, I thank my family and friends for their constant encouragement and support. My family has always instilled in me the values of hard work and humility, while my friends keep me motivated and positive. I am very thankful to be surrounded by them and attribute any and all of my accomplishments to them.

Table of Contents

List of Figures and Tables

FIGURES

TABLE

Introduction

The discovery of hydrocarbon accumulations in carbonate lacustrine microbial reservoirs in the pre-salt of the South Atlantic has motivated the search for analogs that could provide perspectives on the nature and origin of initial porosity in these reservoirs. Although previous efforts have mapped spatial patterns of extant microbial lacustrine systems on a large (km) scale (e.g., Harris et al., 2013), described general aspects of environments and facies models and the variability of microbial lacustrine systems (e.g., Gierlowski-Kordesch, 2010; Wright, 2012; Della Porta, 2015), and explored the abiotic and biotic (e.g., microorganism) influences on the formation of microbialites (e.g., Riding, 2000; Wright, 2012; Wright and Barnett, 2015; Harwood Theisen et al., 2015), the details of the origins and controls of organic matter source, abundance, and growth habit on depositional textures and associated pore attributes of microbialites are less well constrained. Seldom do geologic studies bridge the gap between organic matter controls on core- or thin-section-scale carbonate textures and associated pore attributes within microbialites.

Microbialites are defined as "organosedimentary deposits that have accreted as a result of a benthic microbial communities trapping and binding sediment or forming the locus of mineral precipitation, or both" (Burne and Moore, 1987, p. 241-242). Microbial mats rarely are preserved in the fossil record, because they are dominantly organic; as a result, evidence into the formation of living microbial mats typically is indirect (e.g., morphology, organic biomarkers, and stable isotopic fractionation) (Dupraz, 2011). Accretion and preservation of microbial carbonates relies principally on early lithification, which can be either biologically (biotically) or environmentally (abiotically) dependent (Riding, 2000). Recent microbialites occupy a very broad range of environments with waters of widely differing chemistry, including marine, hypersaline, alkaline,

freshwater, and even continental environments. Microbialites are common in hypersaline environments, because microbial communities are able to thrive within high salinity environments where predators are rare to absent (Awramik, 1992; Riding, 2006). Microbialite fabrics can reflect any changes in environmental conditions (i.e., water chemistry) that influence microbial metabolism or the saturation state of water with respect to carbonate, or both. Consequently, one of the possible influences on the dynamics of microbialite growth (and hence textures and porosity) is abundance and morphology of organic matter (Riding, 2000).

Microbialites can be classified into four common types based on their cm-scale macrofabrics (Burne and Moore, 1987; Riding 2000), but most common are stromatolitic and thrombolitic fabrics. Stromatolites consist of an internally laminated and thinly layered fabric, whereas thrombolites are composed of irregular clots that can elongate into branches (Riding, 2000). Both macrofabrics exhibit a range of finer-scale internal microfabric, and distinct pore attributes.

To provide perspectives on syn-depositional pores in ancient carbonates (including pre-salt reservoirs), this project characterizes microbialite deposits of a recent lake on Long Cay, Crooked-Acklins Platform (CAP), southern Bahamas. The ultimate goal of this actualistic study is to understand the influences of organic matter source, abundance, and growth habit on carbonate depositional textures and associated pore attributes by characterizing both microscopic and macroscopic fabrics of Holocene microbialites. Results from both lab and field analyses at several scales reveal variation in fabric and preservation of porosity as a function of the growth habit and presence of abundant organic matter. Collectively, results can provide insight into the variability and characteristics of pore attributes that are controlled by comparable organic matter source, abundance, and growth habit within ancient microbialite deposits in which organic matter is not

preserved. Understanding of depositional pore volumes, size, abundance, distribution, and connectivity within microbialites can form the foundation of conceptual and geological models, as pore attributes in analogous reservoirs can be influenced strongly by the original fabric of the rock.

Background

Study Setting

Long Cay is located on the CAP in the southern Bahamas. CAP, covering an area of approximately 2,600 km^2, consists of a shallow-marine isolated carbonate platform, and is ringed by Long Cay to the west, Acklins Island to the east, and Crooked Island to the north. Long Cay includes a variety of extant hypersaline, alkaline lacustrine systems, with unlithified microbial mats, lithified microbialites, or no microbial growth. The focus of this study is Windsor Point Salt Pond, a small, elongate, hypersaline, alkaline lake parallel to the coastline on the southeast flank of Long Cay (Figure 1; ~22˚33'N, 74˚22'W). It is considered a cutoff lagoon that formed by aggradation or longshore progradation of the flanking beach ridges (cf. Park Boush et al., 2014). Its long axis is approximately 2.5 km in length, and no more than 0.25 km across, bounded by beach ridges to the east and impermeable Pleistocene bedrock to the west. The lake receives inflow from runoff during rainfall, by overwash related to extreme events, and through the permeable beach ridges. The lake is characterized by net evaporation, and water levels vary with rainfall, but water depth is shallow (less than 1 m). The lack of continuous, direct connection to either groundwater or marine water likely controls the hypersaline and organic-rich nature of the lake (cf. Park Boush et al., 2014). As a result of saline recharge, evaporation, and meteoric precipitation, the water chemistry of this lake likely changes continuously, but systematic monitoring was beyond the

scope of this study. One measurement revealed salinity of 89 parts per thousand, and further tests revealed a high pH of 9.46, verifying the lake water was both hypersaline and alkaline, at least at that time.

Previous studies have documented that the complex Holocene regional climate history influenced the variation of deposits found within broadly comparable lacustrine systems in the Bahamas. A widespread dry period in the Caribbean occurred from 3200 to 1500 years before present (ybp), followed by a more mesic climate (Kjellmark, 1996), which led to tropical hardwood vegetation (Dix et al., 1999). Many semi-protected coastal embayments in the Bahamas were closed by ~740–700 ybp possibly due to changing coastal oceanographic and depositional patterns related to a regional change in climate (Dix et al., 1999). Closure formed numerous restricted, saline ponds with highly variable salinities and progressive isolation from marine influence (Dix et al., 1999). In the last 200 years, organic productivity has dominated many lakes as carbonate accumulation has shut off, a dynamic interpreted to be related to increased eutrophication (Dix et al., 1999).

Sample Collection, Preparation, and Analyses Methods

Field Sampling Sites & Collection

High-resolution (QuickBird, 240 cm multispectral and 60 cm panchromatic pixels) satellite images of Windsor Point Salt Pond provided spatial context for sampling prior to fieldwork. On the basis of the remote sensing data analysis, fourteen east - west transects across the lake sampled the range of benthic variability, focusing on observations of bathymetry and bottom types, and their spatial variability. Forty unlithified mats collected in glass jars, plastic vials, and plastic containers, 12

whole microbialite samples wrapped in aluminum foil to prevent contamination by foreign organic matter or other materials, and 30 surface sediment samples collected in plastic vials captured the range of variability and characterized fabrics of bottom types within the elongate lake. Eight shallow push cores (corresponding to decompacted thicknesses up to 93 cm) sampled the stratigraphic evolution of the lake. All samples provide data and insight on microbialite fabrics from use in thin-section analysis, gas chromatography/mass spectroscopy (GC/MS), X-ray diffraction (XRD), and nuclear magnetic resonance (NMR) analyses, radiocarbon age dating, and computed tomography (CT) scan production. To evaluate water chemistry, four water samples collected in the field measured both the salinity and pH of the lake waters.

Thin Section and Microbialite Hand Samples

Observations and descriptions of hand samples and thin sections under a petrographic microscope provide insights into depositional textures and associated pore attributes. This study uses "depositional texture" to refer to use of classification of Dunham (1962) for granular material and Embry and Klovan (1971) for bound components. "Fabric" herein is based on the Della Porta (2015) classification of non-marine carbonate rocks and which utilizes texture, orientation and alignment of components, the presence or absence of cement, microbial growth characteristics, and pore attributes (e.g., expanding on Dunham, 1962, Embry and Klovan, 1971, and Wright, 1992). Pore type classification is modified from Choquette and Pray (1970), Lucia (1995), Rezende et al. (2013), and Della Porta (2015). Macrofabrics are fabrics on a cm to mm scale, whereas microfabrics are on a petrographic scale (mm to microns). Thin sections (n = 142) produced for each of the spectrum of bottom types (i.e., unlithified living microbial mats, lithified

microbialites, and organic-rich sediment) were used to observe, describe, and identify fabrics, relate textures with pore attributes and organic matter, classify pores, and quantify porosity. Six cut, slabbed, and polished microbialite samples (up to 30 cm tall) reveal macroscopic microbialite fabrics, and impregnated shallow push cores illustrate lake stratigraphy.

GC/MS

Biomarkers are organic compounds (primarily lipids) synthesized by once-living organisms, and can be preserved in sediments and sedimentary rocks (Peters et al., 2005). Different organisms synthesize different types of molecules, thus biomarkers in a rock can be used to infer what organisms were present at deposition, and thus can provide insights into paleoenvironments and specific microbial metabolisms (Peters et al., 2005). As molecules break down during diagenesis, molecular structure in preserved biomarkers can be used to determine the maximum diagenetic temperature and pressure (thermal maturity) experienced during burial in a rock or oil. There are a variety of biomarkers that can aid in determining the source and maturity of the organic matter. In particular, polycyclic structures, hopanes and steranes are used widely as sedimentary fingerprints for bacterial and eukaryotic source inputs (Talbot et al., 2003; Volkman, 2005). Various factors, including the type of organic matter input, redox potential during sedimentation, bioturbation, sediment grain size, and sedimentation rate influence the quantity and quality of preserved organic matter, which in turn affects the detectability of various biomarkers (Peters et al., 2005). GC/MS combines two techniques to analyze biomarkers: retention time in the GC identifies the chemical structures of biomarkers and the MS breaks these structures into unique fragmentation patterns. Different suites of biomarkers were identified based on their specific ion-

mass to ion-charge (m/z) number, relative retention time, and comparison with literature data. To ensure the correct identification of compounds, these fragmentation patterns, retention times, and m/z numbers were cross checked against a database created by the National Institute of Standards and Technology as well as previously published fragmentograms.

To analyze samples, a mechanical ball mill grinder crushed three samples from each end-member microbialite fabric (a total of nine samples) to powder for a duration of ~30 minutes per sample at 225 rpm. Solvent-washed stainless steel jar and balls prevented contamination between crushing of different samples. Five grams of the powdered sample in a Teflon tube along with 22.5 mL of dichloromethane (DCM) and 2.5 mL of methanol (MeOH) were placed in a microwave-accelerated reaction system (MARS) to extract organic material from the sample. Vacuum filtering of samples, after the 40 minute extraction, retained only liquid extracts. To remove any elemental sulfur, four pipette column volumes of HCl and deionized water filtered through a glass pipet containing activated copper (Cu), plugged with wool. The liquid extracts from each sample then reacted with the activated Cu by pipetting a sample of ~20 mL into the top of the pipette filled with Cu. Once the sample finished percolating through the copper column, four pipette column volumes of DCM ran through the column. All filtered extracts and DCM, caught in a 40 mL glass vial, were evaporated down to dryness using a TurboVap, and then brought back up to 1 mL with DCM. Eight mL of MeOH with 5% HCl added to the remaining 0.5 mL samples sat overnight at 70˚C and, once again, were evaporated down to dryness. The methylated samples along with 5 mL of hexane in each sample were then transferred to 1.5 mL sized GC vials for analysis at the University of Kansas. All glassware used during preparation for GC/MS analyses were combusted over night at 430 ˚C and solvent washed before use to remove any and

all contaminants.

Quantitative Three-Dimensional Pore Characterization

Pore attributes of microbialites are very complex and difficult to describe using traditional methods (e.g., general attributes and petrography), so volumetric techniques, such as CT-scans, enhance three dimensional understanding of pore attributes. CT-scans provide quantitative data on bulk porosity of microbialites and reveal zones with fabric differences related to changes in geometry, connectivity, and associated porosity. CT-scans of four microbialite samples, completed at CoreLab in Houston, Texas, have image resolution of 0.45 mm (limiting the precision of pore volumes to be 450 μm or larger), well into the macroporosity domain (Cantrell and Haggerty, 1999). These data were converted to Society of Exploration Geophysicists Y (SEG-Y) file format for use in Petrel software to segment two-dimensional (2D) horizons as well as for input into Avizo Fire (FEI Company, Inc., part of Thermo Fisher Scientific, Inc.), an advanced 2D and 3D analysis software. Avizo Fire delivers visualization of pores and data pertaining to pore size and pore size distribution. The data consist of 355 slices with a voxel size of 0.3 x 0.459 x 0.459 mm. Image analysis software, JMicroVision, quantified macroporosity, defined as pore body diameters of 10 μm or greater (Cantrell and Hagerty, 1999), within microbialite samples, by using the extracted 2D horizons in the X, Y, and Z planes (n = 20). In addition, JMicroVision, measured and quantified microscale porosity, pore body diameters less than 10 μm (Cantrell and Hagerty, 1999), in microbialites from photomicrographs (n = 30). With the *Background* tool in JMicroVision, pore space as well as organic matter were manually extracted by selecting all pixels with digital values interpreted to represent pore space and organic matter, respectively, within photomicrographs and

2D macro CT-scan horizons. This tool then allowed for the calculation of total selected pixels versus all pixels within the entire image resulting in selected pixel percentage, which represents pore space.

NMR

NMR is a noninvasive technique that provides quantitative data on bulk porosity and pore size distribution and abundance. In NMR experiments, rock samples are saturated with fluid and placed in a magnetic field and excited by pulses (Brown and Gamson, 1960). Pulses generate an echo train and the echoes decay giving relaxation times (T_2). The initial amplitude of the echo signal indicates the total amount of fluid in the sample or the porosity (ratio of the pore volume to the bulk volume) of the sample (Coates et al., 1999). The measured magnetization decay or T_2 of water molecules within rock pore space deduces information pertaining to pore attributes. The magnetization is due to the spin of hydrogen protons in the water molecules which possess a magnetic moment (Vincent et al., 2011). T_2 distribution reflects a distribution of the volume to surface ratio and includes a shape factor and can be translated to roughly calculate pore size (Dunn et al., 2002). Signals with short T_2 can be attributed to smaller pores, whereas larger pores have long T_2 (Brown and Gamson, 1960). Using this method, it is difficult to capture all macropores as well as pores that are completely isolated so results are as accurate as the limitations allowed for the highly porous samples of this study (Westphal et al., 2005). Similarly, NMR may characterize organic matter as "pores" due to their high water content; as this organic matter likely will not be preserved, and the space will at some point be porosity, this limitation is sufficient for purposes here (Webber et al., 2013).

Eleven core plugs, drilled from three representative microbialites, include a 2.54 cm diameter, an average length of 5 cm, weighed on average 30 g. An oven set at 60˚C dried samples in ~24 hours, or until the weight of each plug did not change with subsequent weighing. Dried samples were then saturated in deionized water for 10 hours using a vacuum until a constant weight was yet again achieved. A displacement method determined the volume of the plugs to give the wet weight of the plugs. Measured values of dried, saturated, and wet weights calculated the pore volume and bulk volume of plugs and roughly estimated porosity. To prevent water loss during NMR experiments, ~100 cm of Teflon tape sealed the saturated plugs. Calculated bulk volumes of core plugs from sample preparation were input into the NMR software and then NMR analyses followed. NMR measurements, completed at the University of Kansas, used a 2MHz Rock Core Analyzer (Magritek Ltd) with the Carr-Purcell-Meiboom-Gill pulse sequence. The measurements had an echo time of 100 μs, inter-experiment times of 17500 ms, and minimum signal to noise ratios for all measurements of 150. Resultant relative amplitudes and T_2 relaxation times from analyses were used to visualize and determine the pore size distribution and the abundance of these pore sizes as decay rates directly indicate the pore size. Generated relative amplitudes were normalized by dividing each relative amplitude by the sum of all relative amplitudes giving the abundance of pore sizes. T_2 relaxation time was then used to calculate pore diameter using the equation $\frac{1}{T_2} = \frac{\rho_2 S}{V}$ (assuming fast diffusion regime), where ρ_2 is the surface relaxivity dependent on lithology and $\frac{S}{V}$ is surface area to volume ratio. Assuming spherical particles, the $\frac{S}{V}$ is 6. Likewise, a ρ_2 value of 5.0 μm/s was selected due to a carbonate lithology and pores being interparticle, primary pores that are dominantly macropores within the microbialites (Choquette and Pray, 1972; Lønøy, 2006; Vincent et al., 2011). Both $\frac{S}{V}$ and ρ_2 are assumed based off of literature from other

rocks so caution should be taken when using these values.

XRD

To evaluate the mineralogy (aragonite versus calcite, which controls diagenetic susceptibility) of the lacustrine carbonate deposits, XRD analyses assessed eight samples. Carbonate spherules, placed into a 1.5 mL vial by sterile tweezers, characterized carbonate mineralogy from a representative unlithified living mat. A dilute solution of 3% hydrogen peroxide removed any organic matter still attached to these spherules. A second crushed and powdered sample, consisting of a ~8 cm^3 portion of lithified microbialite, was transferred to a 1.5 mL vial for analysis. Bulk powder XRD analyses of these samples, completed at the X-ray Crystallography Laboratory at the University of Kansas, identified mineralogy in a diffractometer and in-house interpretation of data results with Eva by Bruker software in the laboratory. The remaining six samples, run at the Chemistry Department X-ray Facility at Wake Forest University, analyzed the mineralogy of microbialites from thin sections at progressively finer scales of 1.0 cm, 1.0 mm, and 0.5 mm. A line focus scanned the cm-scale variations of the carbonates, whereas spot configuration analyzed the carbonate laminations with alternating character within microbialites at scales of 0.5 to 1.0 mm.

Radiocarbon Age Dating

Carbon-13 and carbon-14 (^{14}C) are isotopes of carbon-12. ^{14}C is not stable, as a result continuously undergoes natural radioactive decay. The rate at which ^{14}C decays is constant at a half-life of 5730 years. Measuring the ^{14}C concentration or residual radioactivity of inorganic carbonate samples,

whose ages are not known, yields the number of decay events. By comparing these data with modern levels of activity and using measured half-lives, the date of death of each sample can be calculated. In this study, radiocarbon age dating is used to constrain the rate of growth of microbialites and differences in growth rates among fabrics within microbialites, as well as compares spherule ages in shallow core and living mats to carbonates in microbialites.

Three distinct areas in two different microbialites (six samples) were sampled by mining out ~1 g carbonates using a micro-drill into a glass vial. Carbonates grains within unlithified mats (four samples) were picked out by sterile tweezers and placed in a vial. To remove organic material, a dilute solution of 3% hydrogen peroxide dissolved the organics. Carbonate samples were dated at Woods Hole Oceanographic Institute in the National Ocean Sciences Accelerator Mass Spectrometry (AMS) lab specifically by using a carbonate hydrolysis process following the methods of Gagnon and Jones (1993) (see Appendix III).

Variability of Holocene Lacustrine Deposits

Bottom Types and Surface Sediment

Observations and field mapping reveal that the calcareous microbialites of Windsor Point Salt Pond occur in the shallow lake, in association with a range of bottom types, including unlithified living microbial mats, the calcareous microbialites, and Pleistocene bedrock (Figure 2). These bottom types are distributed systematically within the elongate lake (Figure 3), with clear zonation relative to water depth, and include the following:

Bottom Type 1 – Domal, laminated mats (Figure 2A). This bottom type occurs exclusively at the easternmost margin of the lake, nearest the Holocene beach ridges, and along the western

margin of the lake (Figure 3B, C). It occurs at elevations that would be < ~10 cm water depth at lake-full level (estimated as the elevation of mangroves and lowest grasses), and forms zones up to 20 m wide on both flanks of the lake. The surface of these mats is irregular, and commonly includes cm-scale relief (up to 5 cm) domes separated by v-shaped depressions (related to desiccation; cf. Allen, 1982). Internally, they include a dark, gelatinous texture with mm-scale continuous, wavy laminations parallel to the margins that reflect changes in included disseminated, fine (clay to silt-sized) carbonate content. Petrographic observations suggest that the fine carbonate consists of diatoms, spherules, and other carbonate grains with aragonite mineralogy. This bottom type is comparable to the "pustular mats" of Jahnert and Collins (2013).

Bottom Type 2 - Flat, laminated mats (Figure 2B). Bottom Type 1 transitions laterally into this bottom type, in lake-full water depths of ~8 to ~20 cm, forming zones up to 35 m wide on both margins of the lake (Figures 3B, C). The surface of these mats include extracellular polymeric substance (EPS) associated with their uppermost laminations. Internally, the mats consist of multiple gelatinous, organic-rich laminations with alternating pigments (i.e., yellow to green-pigmented horizons in upper laminations transition into dark brown, maroon, grey, and black-pigmented laminations in the deeper laminations). Overall morphology of mats are flat and parallel, although some laminations are wavy. Carbonate grains within this bottom type are clay to silt size (10s of μm) and petrographic observations reveal the presence of small spherules and subspherical to spherical unidentifiable carbonate grains. This bottom type is similar to the "microbial mats" (during drought stages) as described by Delfino et al. (2012).

Bottom Type 3 - Flat, laminated mats with coarse and abundant carbonates (Figure 2C). Bottom Type 2 gradually progresses laterally within the lake into this bottom type, at distances

approximately 55 m from the eastern flank, and it is present on the western flank of the lake as well (Figures 3B, C). It occurs in lake-full water depths of ~20 to ~60 cm in a zone 35 m wide on the eastern side of the lake and 15 m wide on the western side of the lake. The multi-layer mats are similar to Bottom Type 2 mats, except that they also include abundant and coarse carbonate grains (Figures 4 A, B). Petrographic observations reveal that these carbonates consist mostly of spherules that consist of numerous 10-100 μm-thick concentric laminations with micro-boring or degradation of organic matter in outer laminations. Spherules reach up to 800 μm diameters (Figure 4C); several grains include a competitive growth boundary between two spherules (e.g., Figure 4D), interpreted to indicate competitive *in situ* growth. The spherules include no visible nucleus, but have a cortex of radial aragonite crystals (mineralogy from XRD) (Figure 4E, F). The spherules and other carbonate grains are not distributed evenly within the mats, but instead appear concentrated within certain layers within the mats, where they can coalesce. Spherules with a diameter less than 50 μm are dispersed within the surface layer of EPS, whereas carbonate grains coarsen, coalesce, or both, in deeper regions (~3 cm from the mat-water interface) of the mat. That is, in the upper parts of mats, fine-grained (clay to silt-size) carbonate grains in the yellow to green-pigmented region transition downward to coarser (sand-size) carbonate grains or silt-size grains in the deeper, dark maroon and brown regions of the mat (Figure 4A). In some cases, however, the gelatinous mats have a thin (< 5 mm) calcareous lamination at the surface. This bottom type is roughly comparable to the "microbial mats" of Delfino et al. (2012).

Bottom Type 4 - Calcareous microbialites (Figure 2D). The center of the lake, in the deepest water depths (30 cm up to 60 cm), is occupied by calcareous microbialites, in varying sizes and spatial arrangement in a zone up to 120 m wide (Figures 3B, C). The microbialites are roughly

subcircular, commonly 15 cm in diameter and 15 cm in height, but they can be much larger (~100 x ~25 cm) or smaller (~4 x ~2 cm). Dark, organic-rich granular surface sediment (Figure 2E) or Bottom Type 3 occurs in lows between the microbialites, and is dominated by spherules and, less frequently, skeletal grains. This bottom type is comparable to the "Holocene microbialites" of Rezende et al. (2013).

Bottom Type 5 - Pleistocene bedrock (Figure 2F). The bedrock occurs ~75 m from the western flank of the lake and is exposed for a width of 20 m in water < 30 cm deep (Figure 3B, C). The impermeable rock consists of cemented ooid grainstone and in some cases is encrusted by calcareous microbial deposits.

Microbialite Components, Textures, and Fabrics and Associated Pore Attributes

Although the non-calcareous mats common near the margins of the lake are interesting, the focus of this study is on the distinct calcareous accumulations most common near the center of the lake. The components, microfabrics, and macrofabrics of these microbialites contrast with those of granular material, and as a result, pores include distinct geometries and complex network connection patterns (Ahr, 2008; Rezende et al., 2013).

By analogy with granular sediment in which the arrangement and sizes of grains make up a rock's texture (e.g., Dunham, 1962) or growth fabrics which define textures (Embry and Klovan, 1974), several microscopic components make up the microbialites. These components include: (1) fibrous high-Mg calcite associated with abundant organic matter progressing from weakly to completely calcified (Figure 5A, B, C), (2) clear fibrous and botryoidal aragonite that is either discontinuous (distinct botryoids) or forms more continuous laminae (coalesced botryoids) (Figure

5D, E) and occasionally is bored and partly to completely micritized (Figure 5F), (3) sub-mm wavy micritic laminae parallel to margins intimately associated with clear fibrous botryoids (Figure 6A), (4) rare sedimentary particles such as forams and mollusks (Figure 6B), (5) particles that are clearly angular, fitted fragments of the other components (e.g., a breccia) (Figure 6C), (6) intervals of homogeneous to clotted micrite, with no evident internal structure (Figure 6D), (7) rare instances of spherules that are 50 to 800 μm in diameter. These features can be amalgamated (Figure 6E) or micritized within the microbialites (Figure 6F).

Petrographic observations reveal that these components collectively form three end-member microscopic fabrics, with distinct pore types and abundances (Figures 7-8). *Fabric 1* includes intimately associated organic matter and fibrous high-Mg calcite and, less commonly, breccia (Figure 7B). It has high porosity (mean porosity = 53 ± 5%, n = 30), which can be classified as intra-fibrous (IF), breccia (BR), and vuggy (VUG) pores (Figure 8A, B). This fabric includes a spectrum of phases of calcification, from weakly to completely calcified (cf. Figure 5A, B, C). In contrast, *Fabric 2* is characterized by alternating mm (to sub-mm)-scale laminations of the laminated micrite, and the clear fibrous and botryoidal aragonite, with the clotted or brecciated micrite between some of the laminations (Figure 7C). Fabric 2 includes both inter-laminar (IL) and breccia (BR) pores, with mean porosity = 40 ± 6% (n = 30; Figure 8C). Finally, *Fabric 3* has dense laminations of micrite and (much less commonly) clear botryoidal aragonite (Figure 7D), and consists of only intra- (WL) and inter-laminar (IL) pores (mean porosity = 12 ± 3%; n = 30) (Figure 8D). Although these three fabrics are recognizable in distinct areas, a complete spectrum among them is evident throughout many microbialites.

Within these Bahamian microbialites, the components and microfabrics (both the end-

members and the gradations between end-members) make up macrofabrics visible with the naked eye in slab or core (Figures 9, 10). Macrofabrics range from stromatolitic (laminated; Figure 9A) to thrombolitic (clotted; Figure 9B) to a bulbous outer coating consisting of tight, micritic laminations (Figure 10A, B). Averages of data from 12 microbialites suggest that the stromatolitic macrofabric comprises approximately 25% of the macroscopic features of the Holocene microbialites, thrombolitic macrofabrics makes up the greater part at ~60%, and ~15% is the outer laminated coating. The stromatolitic intervals include oriented, wavy to horizontal, parallel carbonate and organic-rich laminations. Growth patterns within this macrofabric also create digitate textures (Figure 10B). Consequently, stromatolitic pores include both inter-laminar (IL) and digitate (DG) pore classes (Figure 10C, D). In contrast, the thrombolitic macrofabric includes interconnected and morphologically irregular branches (Figure 10B), with chaotic (clotted) fabric resulting in branching (BRA) pores, which are elongate and typically form irregular shapes (Figure 10C, D; comparable to the observations of thrombolites of Rezende et al., 2013). Finally, the bulbous outer coating includes a mm-scale mammillary outer appearance superimposed on vertically elongate cm-scale bulbs ranging, and internally consists of numerous continuous 100-μm thick, tight micritic margin-parallel laminations. In comparing with petrographic observations, although Fabric 3 corresponds directly to the bulbous macrofabric of the outer coating of the microbialite, Fabrics 1 and 2 are not correlated directly to a specific macrofabric. Instead, Fabrics 1 and 2 are found in varying abundance and configuration within both the stromatolitic and the thrombolitic macrofabrics (cf. Figures 9, 10).

In association with inter- and intra-textural changes, porosity within the microbialites varies at several scales; pore space is filled with microbial biomass (organic matter), remains open, or,

less commonly, includes sediment infill. To quantify porosity and characterize heterogeneity of pore geometries and networks, 2D and 3D reconstructions and analyses included macro CT-scans of macropores, NMR of macro to micropores, and petrography of micropores.

At the largest scale, the average macroporosity of entire microbialites (calculated from macro CT-scans in JMicroVision) ranges from 41 to 48% (mean = 43 ± 3%; n = 20 (e.g., Figure 10C, D)). Avizo Fire explored and analyzed microbialite pore properties in three dimensions. Segmentation tools allowed for accurate identification of rock volumes versus pore volumes and extraction of these features and built-in measurement and statistical tools quantified pore size distributions. A histogram of pore size distribution generated from a representative Holcoene microbialite revealed pores with a log-normal size frequency distribution, with a mode between 1-10 mm^3 (Figure 11).

NMR measurements of core plugs from the microbialite confirm the high porosity associated with these microbialites at the core plug scale (mean porosity = 59 ± 6%; n = 11) (Table 1). Pore size calculations from NMR T_2 relaxation measurements from 11 core plugs (each of which included two or more fabrics) from three different microbialites also reveals that the microbialite pore system is more complex than just a single pore size. The microbialite pore systems include a bi-modal distribution of pore sizes, yet, macropores contribute the most to the overall pore volume (Figure 12). Recall that macropores have pore body diameters 10 μm or greater, whereas micropores have pore body diameters less than 10 μm (Cantrell and Hagerty, 1999). An abrupt end to curves at larger pore sizes (e.g., Figure 12) suggest that full decay or relaxation may not have occurred during experiments. As a result, larger pores may not be captured in the T_2 data, but overall porosity from T_0 was not compromised.

There are advantages and disadvantages to each analytical method for determining porosity, due to their ability to utilize different sample sizes and to capture different scales of pore sizes. As a result, porosity estimates among the three methods illustrates variability. At the largest scale, macro CT-scans have a resolution (0.45 mm) that limits the capability to include micropores that are captured within the NMR measurements. In addition, porosity calculated from macro CT-scans includes entire microbialites (10s of cm-scale) but only from 2D horizons. In contrast, NMR includes bulk volumes of microbialites, but only at a core-plug (2.54 cm in diameter and ~5 cm in height) scale. Consequently, NMR measurements do not capture vuggy pores larger than a size that would make the plug mechanically unstable. Similarly, organic matter that may still remain within core plugs may be calculated by the NMR as pore space due to its high abundance of water. Finally, at a microscale, photomicrographs (2D representations) allow for the examination of pores and their relations to rock fabrics, which is harder or impossible to do with the other analytical methods.

Source, Abundance, and Growth Habit of Organic Matter within Holocene Microbialites

GC/MS analyses of biomarkers within Holocene calcareous microbialites reveal a distribution of short chain fatty acids (C_{15}, C_{16}, C_{18}). This distribution is thought to be representative of a community dominated by bacteria, rather than algae, higher plants or animals (Peters et al., 2005) (Figure 13) and provide evidence that this organic matter is fresh and not necessarily the organic matter present at the time of microbialite formation. The source of organic matter (bacterial communities) is similar among all three end-member fabrics, but there is an order of magnitude more extractable organic matter compounds in Fabrics 1 and 2 compared to Fabric 3. Fabric 1

organic matter contains a broader suite of compounds (i.e., it is a more complex community of bacteria), it preserves more short chain fatty acids, or both compared to Fabrics 2 and 3. This observation is consistent as Fabrics 2 and 3 both include dense, tight micritic laminations and botryoidal aragonite, therefore, organic matter and pore space are less than in Fabric 1. The organic matter from all fabrics within microbialites shows no evidence for the products of diagenesis or signs of Archaea as the measureable compounds are indicative of only bacterial communities.

Organic matter in microbialites consists of filamentous microorganisms, and carbonates precipitating in association with these microorganisms can be associated with fabrics that reflect and preserve the shrub-like (radial growth habit) morphology of the microbial community (Figure 14; cf. Figures 5A-C, 8A). The filamentous microorganisms presumably are photosynthetic cyanobacteria, based on their yellow to green pigment and elongate, filamentous morphologic characteristics (Harwood Theisen et al. 2015), but more study (e.g., additional SEM, EDS, petrographic, and genomic analyses) is needed (and underway) to test this interpretation (Omelon et al., in prep.). In addition, organic matter color can be used to estimate thermal maturity, but that was not completed in this particular study.

In addition to calcium carbonate and organic matter dominated by bacteria, energy dispersive spectroscopic (EDS) mapping within the upper portion these microbialites reveals that magnesium (Mg) and silica (Si) occur, mostly within Fabric 1 (Figure 15). The areas of enhanced Mg and Si abundance appear as elongate, fibrous patches in association with the organic matter. Notably absent in these areas is aluminum (Al), however, suggesting the presence of Mg-silicates, probably as a gel.

Lake Stratigraphy

Although the focus of the study was not on the evolution of the lake, eight shallow cores reveal the shallow stratigraphy and the possible geological expression of bottom types, and include several sediment types not expressed on the extant surface. All eight cores are generally similar (i.e., organic-rich laminations cap carbonate and evaporite- and carbonate-rich sediment).

In one representative core (Figure 16) collected within the Bottom Type 3 zone, the sediment at the base (from 79 to 34 cm compacted depth) makes up Unit 1 (U1) and is composed dominantly of gypsum blades (Figure 16C) up to one mm across their long axis. These evaporites are associated with carbonate mud, rounded to sub-rounded peloids, and skeletal grains (whole and fragments) of marine organisms (e.g., mollusks, forams, and *Halimeda)* up to 5 mm long (Figure 16D. Mm to sub-mm compacted horizontal organic-rich laminations also occur sporadically throughout this section. Upcore, Unit 2 (U2; Figure 16) extends from 33 to 17 cm, reveals sediment similar to the adjacent unit below, except that evaporites are rare to absent. Calcareous mud and rounded to sub-rounded peloids and skeletal grains, with sporadic mm- to sub-mm-thick horizontal compacted organic-rich laminations, make up this unit (Figure 16E). TOC is generally higher in U2 than U1 (means of 12% versus 5%, respectively; Figure 16A) From 16 to 3 cm depth, the upper unit of the core (U3) illustrates well-developed alternating mm-scale wavy to horizontal laminations of carbonate-rich and organic-rich layers, with spherules embedded in the organic-rich laminae (Figure 16F). The uppermost region in the < 3 cm below the sediment-water interface is dominated by organic-rich laminations (total organic carbon (TOC) reaches up to 13%) with rare carbonate precipitates (Figure 16A, B).

Radiocarbon Age Dating

One striking aspect of many pre-salt reservoirs is the thick accumulations of microbialites that seem to grow very rapidly. However, the rates of growth are largely unconstrained in the stratigraphic record. Radiocarbon dating from two of these Holocene microbialites constrain the rates of growth of these microbialites. Radiocarbon dating from one representative microbialite confirms that growth was initiated at least 1,720 ± 20 ybp and its last calcareous growth stages occurred around 725 ± 15 ybp (Figure 17A). Unpublished data (T.J. Waller, Anadarko Petroleum Corporation, personal communication, 2016) suggests similar ages for other microbialites from this lake. These ages provide an overall average growth rate of approximately 0.25 mm/yr for 1000 years, but denser carbonate areas near the base grew faster, at a rate of ~0.43 mm/yr.

In addition to the dates from calcareous microbialites, radiocarbon dating of carbonate grains (spherules) within a core sample, from 5 cm below the surface in the center of the lake, returned an age of 845 ± 15 ybp (Figure 17B). A representative unlithified mat between microbialite heads suggests that carbonates are older progressively deeper within a mat (610 ± 25 ybp down 3 cm to 635 ± 20 ybp) (Figure 17C). In contrast, the carbonates within mats on the margins of the lake are younger (140 ± 25 ybp) than these lake-central carbonates (Figure 17D); recall that these sediments were finer as well.

Discussion

Influence of Organic Matter on Characteristics of Windsor Point Salt Pond Deposits

Windsor Point Salt Pond includes deposits with a variety of components, textures, and fabrics that likely would influence ultimate petrophysical (phi/k) character. These elements represent a range

of scales of heterogeneity. Within the microbialites, the three end-member microfabrics that occur in varying amounts in the thrombolitic, stromatolitic, and bulbous outer coating macrofabrics include unique textures and pore attributes (summarized in Figure 18).

Microfabrics are associated intimately with one another, from the scale of a set of laminae to a thin section, to an entire microbialite, and there is a spectrum between the end members. The influence of organic matter on the creation of fabrics may be caused by changes in organic matter source, abundance, and growth habit. Within these Holocene microbialites, the source of organic matter for all fabrics consists of fresh organic matter dominated by bacterial communities with the absence of algae or higher plants or animals, and so (at the resolution of our data), organic matter source does not appear to play a role in creating differing fabrics. Genomic characterization could provide additional insights, however, it is beyond the scope of this study.

Instead of the source of organic matter, the abundance, complexity, and growth habit of organic matter appear to play essential roles in creating the distinct carbonate textures and associated pore attributes at multiple scales (Figures 5, 6, 14, 15; summarized in Figure 18). For example, at the smallest scale, carbonate precipitation associated with filamentous (and presumably photosynthetic, see above) microorganisms can produce microbialite fabrics at a larger scale (Harwood Theisen et al. 2015). The greatest abundance of these microorganisms creates fibrous micritic (high-Mg calcite) carbonates (Fabric 1). In this study, the preserved range of stages of calcification of the fibrous micrite, from incipient (Figure 14) to partly (Figure 5A, B) to completely (Figure 5C) calcified, is consistent with an interpretation that carbonate precipitation around filamentous organisms creates the microfabric end member Fabric 1 (i.e., elongate and fibrous micrite perpendicular to the margin). Within this fabric, abundant organic matter can be

coated by calcareous precipitates, which, as organic matter decays, could result in intra-fibrous porosity and even carbonate breccia porosity. Carbonate precipitation in this scenario most likely resulted from two closely linked microbial metabolisms: 1) an initial photosynthesis stage, which would lead to nucleation and *in situ* precipitation of carbonates followed by 2) continued carbonate precipitation due to heterotrophic activity (e.g., Omelon et al. 2013).

In contrast, less abundant (or even absent) organic matter may favor the precipitation of aragonite botryoids and dark micritic laminations that together make up laminated parts of Fabrics 2 and 3. These laminated intervals of Fabrics 2 and 3 are broadly similar, yet, Fabric 3 includes less pore space due to denser laminations and botryoids, and absent to rare breccia. Botryoidal aragonite grows on fixed substrates (Aissaoui, 1985), so the surface of these dense fabrics most likely are the substrates that facilitate growth (i.e., provide a nucleation point) of botryoids and dark, micritic laminae, perhaps as abiotic precipitates. Fabric 3 essentially forms the bulbous outer coating consisting of dense, tight micritic laminations and botryoids and forms a coating or rim enveloping microbialites. The radiocarbon dating suggests that the youngest microbialite growth phase (e.g., the date of this outer coating) was ~725 ybp, and suggests that the microbialites may no longer be actively accreting carbonate to any notable degree.

Changes in microbialite fabrics appear cyclic, or at least they include repeated alternations of botryoidal, micritic-laminated, fibrous, brecciated, and homogeneous micritic components (Figures 7, 8, 9). These alternations could reflect seasonal (wet-dry), annual (temperature), El Niño–Southern Oscillation (Michelson and Park Boush, 2016), or other cycle. Any (or all?) of these changes could be related to variations in groundwater chemistry, hydrology, or nutrient supply (Kjellmark, 1996), and may impact variations in the relative abundance in biotically

mediated precipitation (or, sources of microbially mediated precipitation) and abiotic precipitates. Similarly, the removal of organic matter (e.g., by oxidation) could weaken the microbialite framework, leading to collapse, and creation of the internal breccia textures.

Ultimately, these microbialites are of late Holocene age, and have seen minimal diagenesis, so ultimate porosity is unknown. Nonetheless, their rapid growth and the presence of Mg-silicates in these microbialites would trap organic matter in the carbonate framework and limit further carbonate precipitation (Wright, 2012), favoring the preservation of the abundant initial porosity. The absence of Al in the Mg-silicate clay prevents it from being replaced by secondary Al-silicate clays, and instead favoring the production of dolomite, silica, and porosity on transformation of the Mg-silicate gels or minerals (Wright, 2012). So, it is probable that Mg-silicates would have a strong influence on porosity preservation within these deposits, and perhaps generation of secondary porosity during burial (comparable to what has been interpreted in ancient analogs; Tosca and Wright, 2015).

At a larger scale, geologic history of the Bahamas in the Holocene may provide some clues into the character of deposits within Windsor Point Salt Pond. For example, previous studies (e.g., Kjellmark, 1996) have documented a widespread dry period in the Caribbean from ~3200 to ~1500 ybp. This dry period could favor elevated evaporation:precipitation, and raise salinities in the lake, favoring the formation of the evaporites that dominate the basal unit of cores.

An end of this dry period (between 1700-1500 ybp) may have decreased the abundance of evaporites, while concomitantly increasing carbonate sediment accumulation (U2 in the cores). The change to more mesic conditions is roughly consistent with the initiation of microbialite growth within the lake (growth initiated 1,720 ± 20 ybp). This climatic shift may have decreased

salinity or variations in salinity, or modified nutrients, sufficiently to favor growth of microbialites.

Another climate change, returning to drier conditions, occurred approximately 700–740 ybp (Dix et al., 1999), about time of the last stages of growth of the large calcareous microbialites (youngest age dates are 725 ± 15 ybp, but final stages could be slightly younger). This enhanced aridity may not have been as pronounced as the earlier dry period, as no evaporites are present in the younger sediment (e.g., U2 and U3), but may have been sufficient to change salinity or nutrients or alkalinity sufficient to terminate calcareous microbialite growth.

In many central and northern Bahamian lakes, carbonate accumulation was effectively shut-down < 200 years ago, replaced by organic-dominated stromatolite growth (Dix et al., 1999). This observation is inconsistent with results of sedimentologic analysis (Figure 15) and radiocarbon dating (Figure 16) from Windsor Point Salt Pond, which revealed spherules within organic-rich laminations of microbial mats range in age from 845 to 140 ybp in U3 (the uppermost) of cores. This greater age of mat-dominance in the southern Bahamas may reflect a slightly different climate from the northern Bahamas.

The microbialites thus are interpreted to be vestigial lake inhabitants. In this interpretation, not actively growing to any notable extent, but are now being surrounded by unlithified microbial mats, coated by living microbes, and filled with marine skeletal fragments from occasional storm overwash.

Comparison to Lower Cretaceous Pre-salt Carbonate Reservoirs

The pre-salt microbialite reservoirs, located offshore of Brazil and Angola in deep waters of the South Atlantic, extend in age from the Lower Cretaceous to the Neogene. The pre-salt succession

reflects the separation of the South American and African plates in the Early Cretaceous (~150 Ma), associated with rifting and seafloor spreading (Davison, 2007). As rifting spread, basin development progressed from many smaller grabens and lakes ("synrift") to regional subsidence creating lacustrine "sag" deposits (Quirk et al., 2013). The "synrift" strata are dominated by siliciclastics, while the "sag" interval includes substantial lacustrine carbonate deposition and coquinas (Dale et al., 1992).

Although the carbonates within the two different systems precipitated in differing geologic eras, tectonic setting and scales, both the Lower Cretaceous pre-salt carbonates (LCPC) of the "sag" interval and the Holocene microbialites formed in broadly analogous conditions. The similar setting (low energy, stressed, highly alkaline, saline, and silica-rich lakes that generally lack metazoans) led to the formation of comparable deposits, at least in regard to mechanisms for fabric growth and fabric characteristics. During "sag" deposition of the LCPC, carbonates precipitated on the shallow lake floor with morphologies that ranged from spherulitic to shrubby, and included a continuum of intermediate forms creating three distinct sag facies: (1) shrubby, microbially influenced boundstones, (2) intraclast-spherulitic wackestone, packstone, and grainstone, and (3) microbial chert (more common offshore Angola) (Saller et al., 2016). The shrubby microbially influenced boundstones of the LCPC appear to accrete from microorganisms, such as photosynthetic microorganisms, growing toward light that create positive relief structures (Saller et al., 2016). Such interpretations are consistent with the observations from this study that suggest carbonate fabrics within Holocene microbialites reflect and can preserve the shrub-like morphology of a microbial community dominated by filamentous microorganisms (e.g., microbialite fabrics are created when carbonates precipitate around the filamentous

microorganisms such as photosynthetic cyanobacteria with a radial growth habit). Although the presence of microorganisms within the Holocene microbialites is common, botryoidal cement within Fabric 2 laminations suggests evidence of an abiotic origin of microbialite fabrics as well (cf. Wright and Barnett, 2015). The pre-salt shrubs have been suggested to be microbial (Carminatti et al., 2008) and abiotic by others (Wright and Barnett, 2015). The dark, organic-rich irregular laminations within the shrubs are consistent a microbial influence, whereas common fibrous calcite or botryoids in the shrubs not occurring in organic-rich laminations suggests rapid precipitation and suggests a potential abiotic origin (Wright and Barnett, 2015). Both the Cretaceous and Holocene both seem to include evidence of a mix of both abiotic origin and biotic origin.

In terms of fabric characteristics, the two systems are comparable in several ways. The presence of spherules ranging in size from silt to sand, and which appear to grow *in situ*, are common within both the ancient and the modern. However, the mineralogy of spherules differs between the two systems (i.e. aragonite in this Bahamian lake and calcite in ancient; cf. Saller et al., 2016). By analogy with ooids, these differences in mineralogy may be related to energy level. Radial aragonitic ooids are most common in quiet, low-energy settings (Loreau and Purser, 1973) *in situ* generation of spherules within organic mats in Windsor Point Salt Pond (Figures 4D, 16F) may contrast with higher energies of the pre-salt spherules (e.g., they can occur in cross-laminated grainstones).

In addition to similar carbonate grains, Mg-silicates are present within both the LCPC and Holocene microbialites. These gels or minerals can favor preservation of initial pores, which can be substantial in both systems. Primary pores within the LCPC commonly are elongate, creating

branching porosity with high permeability (Saller et al., 2016), similar to the branching porosity found in the thrombolitic macrofabrics of Holocene microbialites.

Carbonates generally precipitated early and formed the framework of the rock (Saller et al., 2016). Although the ultimate preservation of vugs within Holocene microbialites is unknown, vugs are present within both the LCPC and Holocene deposits. Diagenesis is minor within the LCPC reservoirs, possibly because the connate waters during burial were relatively saline and less reactive than freshwater (Saller et al., 2016). In general, spherulites and shrubby microbial components are depositional and adjacent dolomite and minimal recrystallization is diagenetically slightly later. Dolomitization and recrystallization can either reduce porosity (by filling pores) or increase porosity (by creating secondary micro- and macropores) (Tosca and Wright, 2015; Saller et al., 2016). The recrystallization may explain the differing mineralogy between the two systems (i.e., high-Mg calcite and aragonite for this study and calcite for the ancient pre-salt).

Holocene microbialites grow at approximately 0.25 mm/yr on average (Figure 17). These rates are geologically very rapid and consistent with the thick accumulations of microbialites in the LCPC reservoirs, units that seem to grow very rapidly. If microfabrics of the "sag" facies of the LCPC reservoirs have been interpreted to be indicative of seasonally controlled carbonate precipitation along the lake floor, and sag carbonate facies accumulated at average rates of 200 μm/yr to 5 mm/yr (Dorobek et al., 2012). These rates are remarkably rapid for shallow-water carbonate successions, and suggest that much of the sag succession along the conjugate margins of the South Atlantic could have been deposited in one million years or less (Dorobek et al., 2012).

Significance

Conceptual and geologic models are tools routinely used in the oil and gas industry to better understand subsurface reservoirs and reduce exploration risk, and improve field development and business decisions. Typically, data and conceptual models derived from reservoir analog studies are added to the scarce subsurface datasets to generate more accurate representations of the subsurface and model trends of reservoir heterogeneity that would otherwise be impossible. These reservoir analogs are essential in improving the understanding of subsurface reservoir architectures and for the prediction of aspects and behaviors of the subsurface strata, such as in the pre-salt.

Comparison of the Holocene microbialites and LCPC revealed that the Holocene microbialites had similar depositional textures as the LCPC microbial deposits found in inferred analogous depositional environments. Depositional textures control pore networks and overall porosity (Rezende et al., 2013). Thus, the observation and classification of Holocene microbialite depositional textures, in which diagenetic processes are minor, provides a foundation for developing a better understanding of pore evolution (e.g., pore volume, size, abundance, distribution, and connectivity) within the depositional framework (Rezende et al., 2013) of pre-salt reservoirs. These microbially influenced textures and abiotically influenced textures control the initial pore geometry and distribution, which in turn may influence diagenetic alterations of the microbialite rock framework (Morse and Mackenzie, 1990). Understanding these controls can improve the prediction of the fundamental rock characteristics and the petrophysical properties, which is useful for more accurate subsurface reservoir modeling.

Recommendations for Future Work

This study focused on several aspects of the Holocene Bahamian microbialites, including their distribution, porosity and fabrics, and relation to organic matter. Several other follow-up studies could provide useful information, many of which would be related to further biogeochemical study to understand how the lake bottom types formed and how this influenced their micro- and macrofabrics. Several analyses could be utilized. The first is recording the lake water hydrogeochemistry, including parameters such as pH, alkalinity, salinity, temperature, and nutrients. Due to lake levels that fluctuate daily, this quest would require systematic monitoring of lake waters over several months to seasons to build a hydrogeochemical model (Arp et al., 2012). A second approach, stable isotope analyses, could be completed alongside this monitoring. Oxygen and carbon isotope signals in carbonate deposits can be an effective means to distinguish between inorganic and biologically induced precipitation (Solari et al., 2010), and temperature changes. Both would be useful to understand the paleoclimatic and paleoenvironmental history of Windsor Point Salt Pond. Finally, genomic characterization of living microbial mats could provide perspective into the beginning stages of microbialite development (Arp et al., 2012). All proposed biogeochemical work could provide insight into the beginning stages of microbialites and how the climate and environment affect their growth and overall fabrics.

Conclusion

A small (< 1 km^2) and shallow (< 1 m) hypersaline lake in the southern Bahamas includes Holocene microbialites that preserve complex micro- and macroscopic depositional textures and associated pore attributes. Preserved porosity varies considerably at several scales, as a function

of organic matter abundance and growth habit. Macroscopic fabrics within the microbialites range from stromatolitic (laminated) with IL and DG porosity to thrombolitic (clotted) with large BRA pores, with a bulbous outer coating consisting of tight, micritic laminations ("tight" on CT-scans). At a finer scale, petrography illustrates that, within microbialites, three end-member microscopic fabrics include: (*Fabric 1*) organic matter and fibrous micrite associated with high porosity such as IF and VUG pores and, less commonly, brecciation (BR pores) (mean porosity = 53 ± 5%, n = 30), (*Fabric 2*) alternating laminations of mm to sub-mm scale of ropy micrite to clear fibrous and botryoidal cement to clotted/brecciated micrite with IL and BR pores (mean porosity = 40 ± 6%, n = 30), and (*Fabric 3*) dense laminations of micrite with IL and WL pores (mean porosity = 12 ± 3%, n = 30). At all pore scales integrating several analyses, average total porosity for entire microbialites ranges from 43 to 59%. Organic matter within pores is composed of bacterial communities for all three fabrics, with the greatest abundance (highest preservation) in Fabrics 1 and 2. Holocene microbialite fabrics are interpreted to be controlled by these differences in abundance and growth habit of organic matter and, at least in some cases, to the presence of Mg-silicates. Carbonate textures are created by carbonates precipitating around microorganisms and preserved porosity results from the carbonates textures entombing the organic matter, and from Mg-silicates inhibiting further precipitation. Combined, these observations of pore genesis provide a basis for understanding the initial stages of the complex pore evolution evident in ancient carbonates from similar lacustrine environments.

References

AHR, W. M., 2008, Geology of carbonate reservoirs: The identification, description, and characterization of hydrocarbon reservoirs in carbonate rocks: Hoboken, Wiley, 277 p.

AISSAOUI, D.M., 1985, Botryoidal aragonite and its diagenesis: Sedimentology, v. 32, p. 345-361.

ALLEN, J.R.L., 1982, Developments in sedimentology: Sedimentary structures their character and physical basis: Elsevier, v. 2, 663 p.

ARP, G., REIMER, A., REITNER, J., AND PRATT, B.R., 2002, Calcification of cyanobacterial filaments: Girvanella and the origin of lower Paleozoic lime mud: Geology v. 30, p. 579-580.

ARP, G., HELMS, G., KARLINSKA, K., SCHUMANN, G., REIMER, A., REITNER, J. AND TRICHET, J., 2012, Photosynthesis versus exopolymer degradation in the formation of microbialites on the atoll of Kiritimati, Republic of Kiribati, Central Pacific: Geomicrobiology Journal, v. 29, p. 29-65.

AWRAMIK, S.M., 1992, The history and significance of stromatolites, in early organic evolution: Implications for energy and mineral resources, edited by: Schidlowski, M., Kimberley, M.M., McKirdy, D.M., Trudinger, P.A., Springer Berlin, p. 435-449.

BIRD, M.I., AYLIFFE, L.K., FIFIELD, L.K., TURNEY, C.S.M., CRESSWELL, R.G., BARROWS, T.T. AND DAVID, B., 1999, Radiocarbon dating of "old" charcoal using a wet oxidation, stepped-combustion procedure: Radiocarbon, v. 41, p. 127-140.

BROWN, R.J.S. AND GAMSON, B.W., 1960, Nuclear magnetism logging: Journal of Petroleum Technology, v. 219, p. 199-201.

BURNE, R.V., AND MOORE, L.S., 1987, Microbialites: organosedimentary deposits of benthic microbial communities: Palaios, v. 2, p. 241-254.

CANTRELL, D.L. AND HAGERTY, R.M., 1999, Microporosity in Arab Formation carbonates, Saudi Arabia: GeoArabia, v. 4, p.129-154.

CARMINATTI, M., WOLFF, B., AND GAMBOA, L., 2008, New exploratory frontiers in Brazil: Proceedings of the 19th World Petroleum Congress, Madrid, Spain, 11 p.

CHOQUETTE, P.W. AND PRAY, L.C., 1970, Geologic nomenclature and classification of porosity in sedimentary carbonates: American Association of Petroleum Geologists, Bulletin, v. 54, p. 207-250.

COATES, G.R., XIAO, L., AND PRAMMER, M.G., 1999, NMR logging: Principles and Applications, Houston, Halliburton Energy Services.

DALE, C.T., LOPES, J.R., AND ABILIO, S., 1992, Takula oil field and the greater Takula area, Cabinda, Angola: Chapter 13, *in* Halbouty, M.T., ed., Giant Oil and Gas Fields of the Decade 1978–1988: American Association of Petroleum Geologists, Memoir 54, p. 197-215.

DAVISON, I., 2007, Geology and tectonics of the South Atlantic Brazilian salt basins, *in* Ries, A.C., Butler, R.W.H., and Graham, R.H., eds., Deformation of the Continental Crust: The Legacy of Mike Coward: Geological Society, London, Special Publications, v. 272, p. 345-359.

DELFINO, D. O., WANDERLEY, M. D., E SILVA, L. H. S., FEDER, F., & LOPES, F. A., 2012, Sedimentology and temporal distribution of microbial mats from Brejo do Espinho, Rio de Janeiro, Brazil: Sedimentary Geology, v. 263, p. 85-95.

DELLA PORTA, G., 2015, Carbonate build-ups in lacustrine, hydrothermal and fluvial settings: comparing depositional geometry, fabric types and geochemical signature, in Bosence, D. W. J., Gibbons, K. A., Le Heron, D. P., Morgan, W. A., Pritchard, T., and Vining, B. A., ed., Microbial Carbonates in Space and Time: Implications for Global Exploration and Production. Geological Society, London, Special Publications, v. 418, p. 17-68.

DIX, G.R., PATTERSON, R.T. AND PARK, L.E., 1999, Marine saline ponds as sedimentary archives of late Holocene climate and sea-level variation along a carbonate platform margin: Lee Stocking Island, Bahamas: Palaeogeography, Palaeoclimatology, Palaeoecology, v. *150*, p. 223-246.

DOROBEK, S., PICCOLI, L., COFFEY, B. AND ADAMS, A., 2012, Carbonate rock-forming processes in the pre-salt "sag" successions of Campos Basin, offshore Brazil: Evidence for seasonal, dominantly abiotic carbonate precipitation, substrate controls, and broader geologic implications: American Association of Petroleum Geologists Hedberg Conference "Microbial Carbonate Reservoir Characterization" Houston, Texas Abstract, Search and Discovery Abstract.

DUNHAM, R.J., 1962, Classification of carbonate rocks according to depositional texture: *in* Ham, W. E., ed., Classification of Carbonate Rocks – A Symposium: American Association of Petroleum Geologists, Memoir 1, p. 108-121.

DUPRAZ, C., REID, R.P., AND VISSCHER, P.T., 2011, Microbialites, Modern: Encyclopedia of Geobiology, p. 617-635.

EMBRY, A.F. AND KLOVAN, J.E., 1971, A Late Devonian reef tract on northeastern Banks Island, Northwest Territories: Bulletin of Canadian Petroleum Geology, v. 19, p. 730–781.

FROELICH, P.N., 1980, Analysis of organic carbon in marine sediments: Limnology and Oceanography, v. 25, p. 564-572.

GAGNON, A.R. AND JONES, G.A., 1993, AMS-graphite target production methods at the Woods Hole Oceanographic Institution during 1986–1991: Radiocarbon, v. 35, p. 301-310.

GIERLOWSKI-KORDESCH, E.H., 2010, Lacustrine carbonates, *in* Alonso-Zarza, A.M., and Tanner, L.H., eds., Carbonates in Continental Settings: Facies, Environments, and Processes: Developments in Sedimentology, v. 61, p. 1-101.

HARRIS, P.M., ELLIS, J., AND PURKIS, S.J., 2013, Assessing the extent of carbonate deposition in early rift settings: American Association of Petroleum Geologists, Bulletin, v. 97, p. 27-60.

HARWOOD THEISEN, C., SUMNER, D.Y., MACKEY, T.J., LIM, D.S.S., BRADY, A.L., AND SLATER, G.F., 2015, Carbonate fabrics in the modern microbialites of Pavilion Lake: two suites of microfabrics that reflect variation in microbial community morphology, growth habit, and lithification: Geobiology, v. 13, p. 357-372.

JAHNERT, R.J., AND COLLINS, L.B., 2013, Controls on microbial activity and tidal flat evolution in Shark Bay, Western Australia: Sedimentology 60, v. 4, p. 1071-1099.

KJELLMARK, E., 1996, Late Holocene climate change and human disturbance on Andros Island, Bahamas: Journal of Paleolimnology, v. 15, p.133-145.

LØNØY, A., 2006, Making sense of carbonate pore system: American Association of Petroleum Geologists, Bulletin, v. 90, p. 1381–1405.

LUCIA, F.J., 1995, Rock-fabric/petrophysical classification of carbonate pore space for reservoir characterization: American Association of Petroleum Geologists, Bulletin, v. 79, p. 1275-1300.

MICHELSON, A.V., AND PARK BOUSH, L.E., 2016, Paleosalinity records from three lakes on San Salvador Island, Bahamas inferred from preserved ostracode assemblages: 16th Symposium on the Geology of the Bahamas and Other Carbonate Regions: San Salvador Island, Bahamas, p. 124-140.

MORSE, J.W., AND MACKENZIE, F.T., 1990, Geochemistry of sedimentary carbonates: Developments in Sedimentology 48: Netherlands, Elsevier Science Publishers B.V., 705 p.

OMELON, C.R., BRADY, A.L., SLATER, G.F., LAVAL, B., LIM, D.S.S., AND SOUTHAM, G., 2013 Microstructure variability in freshwater microbialites, Pavilion Lake, Canada: Palaeogeography, Palaeoclimatology, Palaeoecology, v. 392, p. 62-70.

PARK BOUSH, L.E., MYRBO, A. AND MICHELSON, A., 2014, A qualitative and quantitative model for climate-driven lake formation on carbonate platforms based on examples from the Bahamian archipelago: Carbonates and Evaporites, v. 29, p. 409-418.

PETERS, K.E., WALTERS, C.C., AND MOLDOWAN, J.M., 2005, The biomarker guide: Volume 2, Biomarkers and isotopes in the environment and earth history, Cambridge University Press, 1107 p.

PURSER, B.H., AND LOREAU, J.P., 1973, Aragonitic, supratidal encrustations on the Trucial Coast, Persian Gulf, *in* Purser, B.H., eds, The Persian Gulf: Springer, Berlin, Heidelberg, p. 343-376.

QUIRK, D.G., HERTLE, M., JEPPESEN, J.W., RAVEN, M., MOHRIAK, W.U., KANN, D.J., AND NØRGAARD, M., 2013, Rifting, subsidence and continental break-up above a mantle plume in the central South Atlantic, *in* Mohriak, W.U., Danforth, A., Post, P.J., Brown, D.E., Tari, G.C., Nemĉok, M., and Sinha, S.T., eds., Conjugate Divergent Margins: Geological Society, London, Special Publications, v. 369, p. 185-214.

REZENDE, M.F., TONIETTO, S.N., AND POPE, M.C., 2013, Three-dimensional pore connectivity evaluation in a Holocene and Jurassic microbialite buildup: American Association of Petroleum Geologists, Bulletin, v. 97, p. 2085-2101.

RIDING, R., 2000, Microbial carbonates: The geological record of calcified bacterial–algal mats and biofilms: Sedimentology, v. 47, p. 179–214.

RIDING, R., 2006, Cyanobacterial calcification, carbon dioxide concentrating mechanisms, and Proterozoic-Cambrian changes in atmospheric composition: Geobiology, v. 4, p. 299-316.

SALLER, A., RUSHTON, S., BUAMBUA, L., INMAN, K., MCNEIL, R., AND DICKSON, J.A.D., 2016, Presalt stratrigraphy and depositional systems in the Kwanza Basin, offshore Angola: American Association of Petroleum Geologists, Bulletin, v. 100, p. 1135-1164.

TALBOT, H.M., WATSON, D.F., PEARSON, E.J., AND FARRIMOND, P., 2003, Diverse biohopanoid compositions of non-marine sediments: Organic Geochemistry, v. 34, p. 1353-1371.

TOSCA, N.J. AND WRIGHT, V.P., 2015, Diagenetic pathways linked to labile Mg-clays in lacustrine carbonate reservoirs: a model for the origin of secondary porosity in the Cretaceous pre-salt Barra Velha Formation, offshore Brazil, *in* Armitage, P.J., Butcher, A.R., Churchill, J. M., Csoma, A.E., Hollis, C., Lander, R.H., Omma, J.E. and Worden, R.H., eds, Reservoir Quality of Clastic and Carbonate Rocks: Analysis, Modelling and Prediction: Geological Society, London, Special Publications, v. 435.

VOLKMAN, J.K., 2005, Sterols and other triterpenoids: Source specificity and evolution of biosynthetic pathways: Organic Geochemistry, v. 36, p. 139-159.

WEBBER, J.B.W., CORBETT, P., SEMPLE, K.T., OGBONNAYA, U., TEEL, W.S., MASIELLO, C.A., FISHER, Q.J., VALENZA, J.J., SONG, Y.Q. AND HU, Q., 2013, An NMR study of porous rock and biochar containing organic material: Microporous and Mesoporous Materials, v. 178, p. 94-98.

WESTPHAL, H., SURHOLT, I., KIESL, C., THERN, H.F., AND KRUSPE, T., 2005, NMR measurements in carbonate rocks: problems and an approach to a solution: Pure and Applied Geophysics, v. 162, p. 549-570.

WRIGHT, V. P., 1992, A revised classification of limestones: Sedimentary Geology, v. 76, p. 177-185.

WRIGHT, V. P., 2012, Lacustrine carbonates in rift settings: The interaction of volcanic and microbial processes on carbonate deposition, *in* Garland, J., Neilson, J.E., Laubach, S.E. and Whidden, K.J. eds., Advances in Carbonate Exploration and Reservoir Analysis: Geological Society, London, Special Publications 2012, v. 370, p. 39-47.

WRIGHT, V. P., AND BARNETT, A.J., 2015, An abiotic model for development of textures in some South Atlantic early Cretaceous lacustrine carbonates, *in* Bosence, D.W.J., Gibbons, K.A., Le Heron, D.P., Morgan, W.A., Pritchard, T., and Vining, B.A., eds., Microbial Carbonates in Space and Time: Implications for Global Exploration and Production: Geological Society, London, Special Publications, v. 418, p. 209-219.

Figures

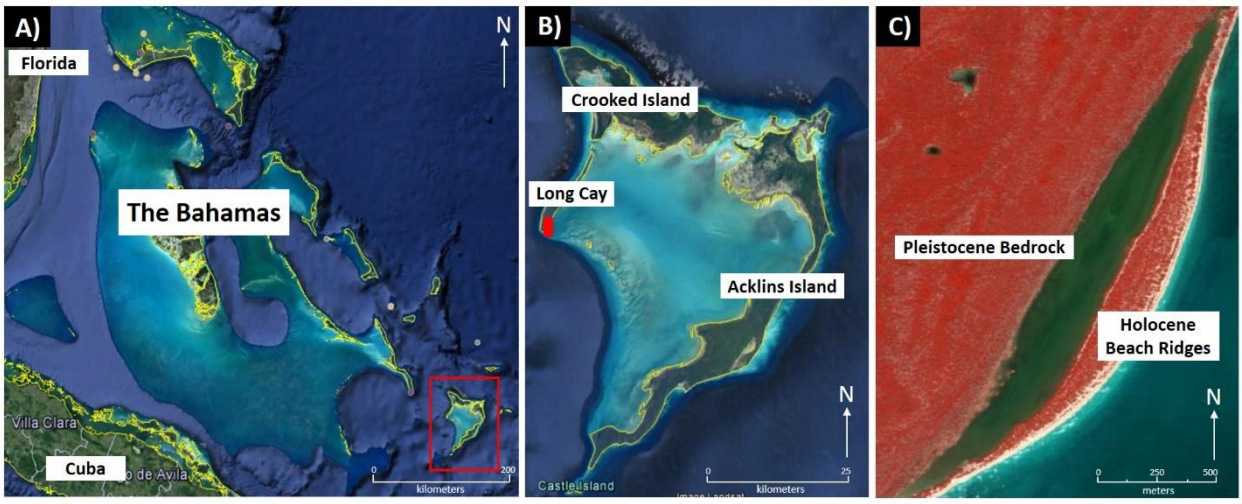

Figure 1: Remote-sensing images of location of Windsor Point Salt Pond on Long Cay on the Crooked-Acklins Platform. Images are copyright GoogleEarth (A, B) and DigitalGlobe (C). A) Location of the Crooked-Acklins Platform (outlined in red), in the southern Bahamas. B) Location of Windsor Point Salt Pond (red rectangle) on the southern tip of Long Cay, Crooked-Acklins Platform. C) Detailed image of Windsor Point Salt Pond, flanked to the west by Pleistocene bedrock, and east by unconsolidated beach ridges.

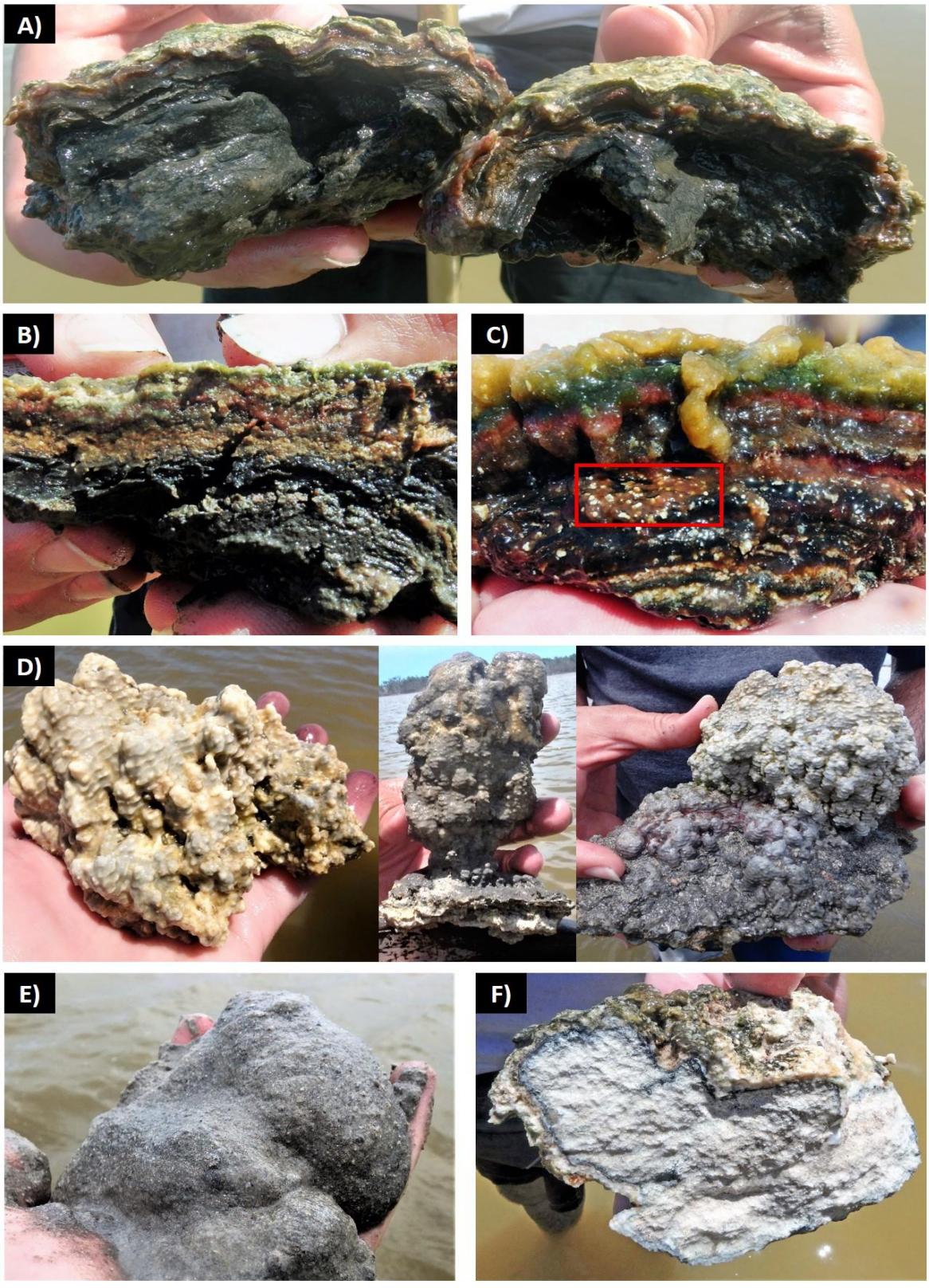
A)
B)
C)
D)
E)
F)

Figure 2: Representative field photos of bottom types in Windsor Point Salt Pond. Hands for scale. A) Bottom Type 1 = domal, laminated mats. B) Bottom Type 2 = flat, laminated unlithified mats. C) Bottom Type 3 = flat, laminated unlithified mats with coarse and abundant carbonates (example of carbonates outlined by red box). D) Bottom Type 4 = lithified calcareous microbialites of varying sizes. These can occur as heads or thin crusts, exposed at the surface or partly to completely buried by organic-rich sediment of Part E. E) Viscous organic-rich sediment, mostly consisting of spherules. E) Bottom Type 5 = Pleistocene bedrock; in this instance, bedrock is encrusted by calcareous microbial deposits (the lighter rim).

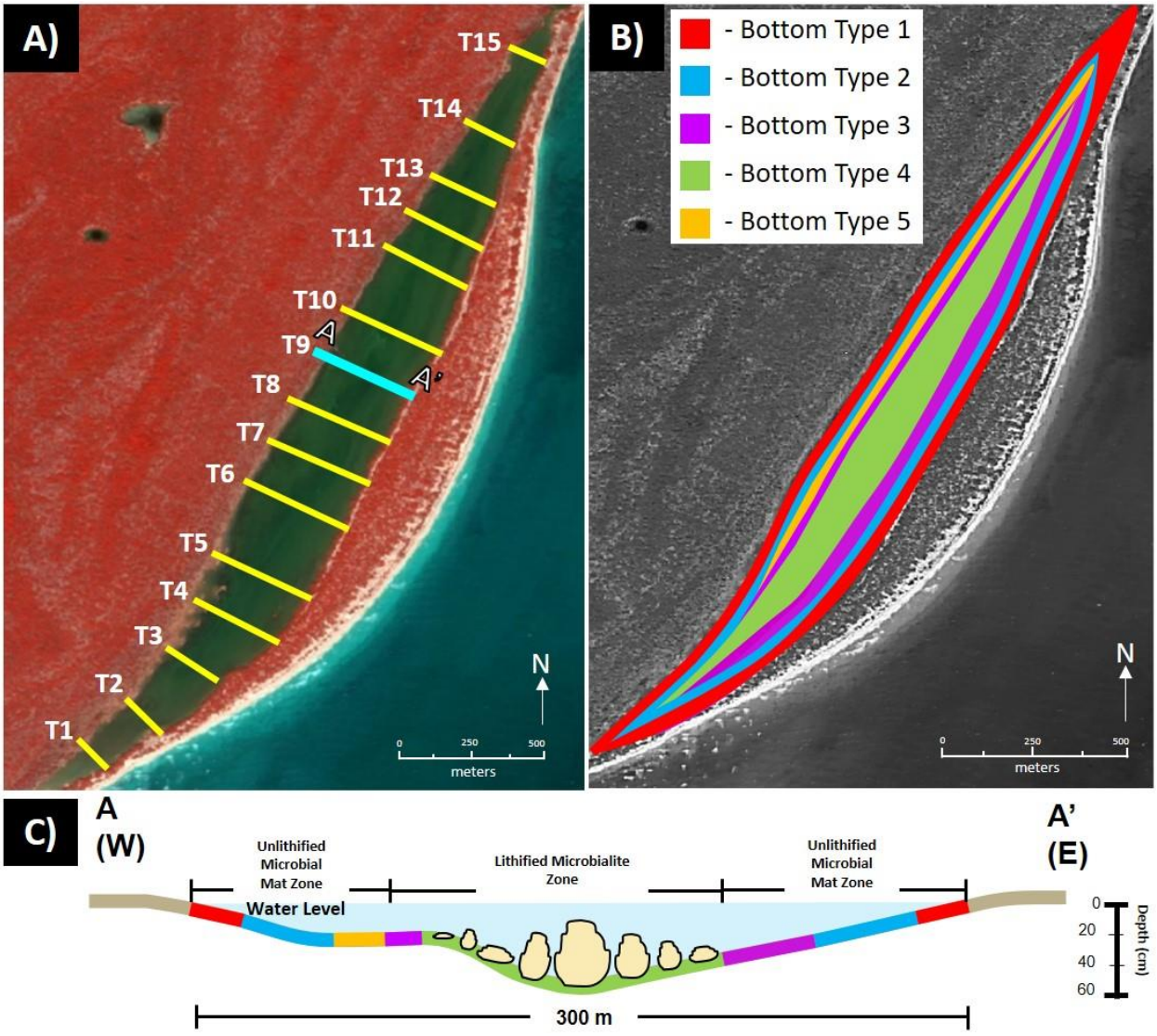

Figure 3: Locations of observations and sampling transects, and distribution of bottom types. A) Remote sensing image of Windsor Point Salt Pond on the Crooked—Acklins Platform with 15 sampling transects represented by yellow lines. Representative cross-section noted at T9 by the blue line and labeled A—A'. B) Summary map of bottom types noted by color. These data reveal systematic shore-parallel distribution of bottom types within the elongate lake. C) Representative cross-section illustrating the changes in bottom type with subtle changes in depth. "Water level" is the approximate level of lake fill, based on the occurrence of mangroves and grasses.

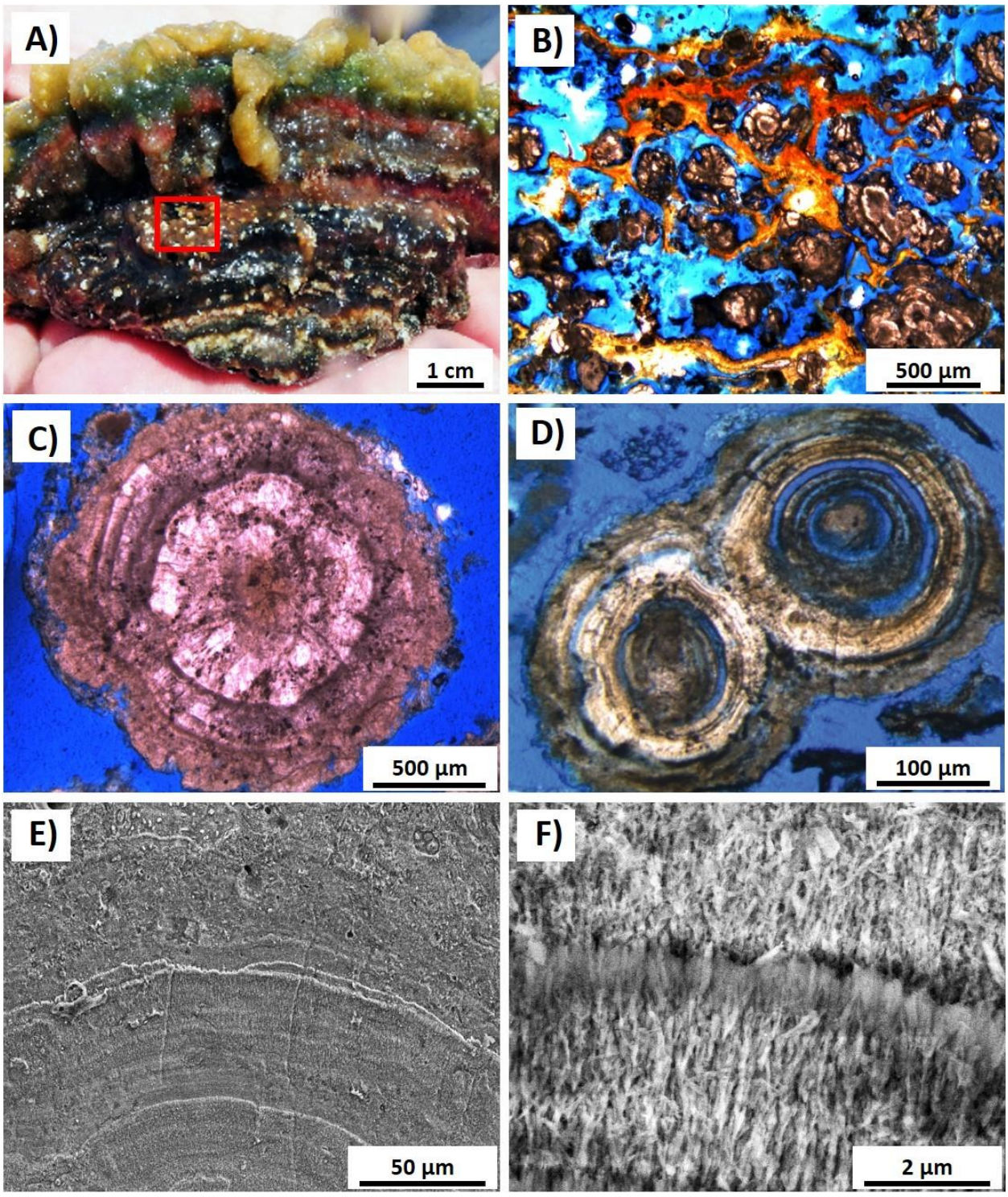

Figure 4: Character of spherulitic sediment. A) Field photo of representative unlithified mat (Bottom Type 3) with organic-rich laminations with light-colored carbonate (spherules), some of which are outlined by red box. B) Thin-section photomicrograph of the carbonates associated with organic matter (orange material in this thin section). Much of the considerable porosity (blue) is

probably the result of desiccation of the mat during thin section preparation. C) Representative spherule. These grains consist of 10-100 μm-thick concentric laminations of radial aragonite crystals with micro-boring or degradation of organic matter in outer laminations, but include no obvious nucleus. D) Thin-section photomicrograph of two spherules that exhibit competitive growth boundaries, suggesting *in situ* growth. Substantial lamina-moldic porosity is also evident. E) SEM image illustrating cortex of concentric laminae; center of grain to the bottom. F) SEM image of radial aragonite crystals (mineralogy provided by XRD).

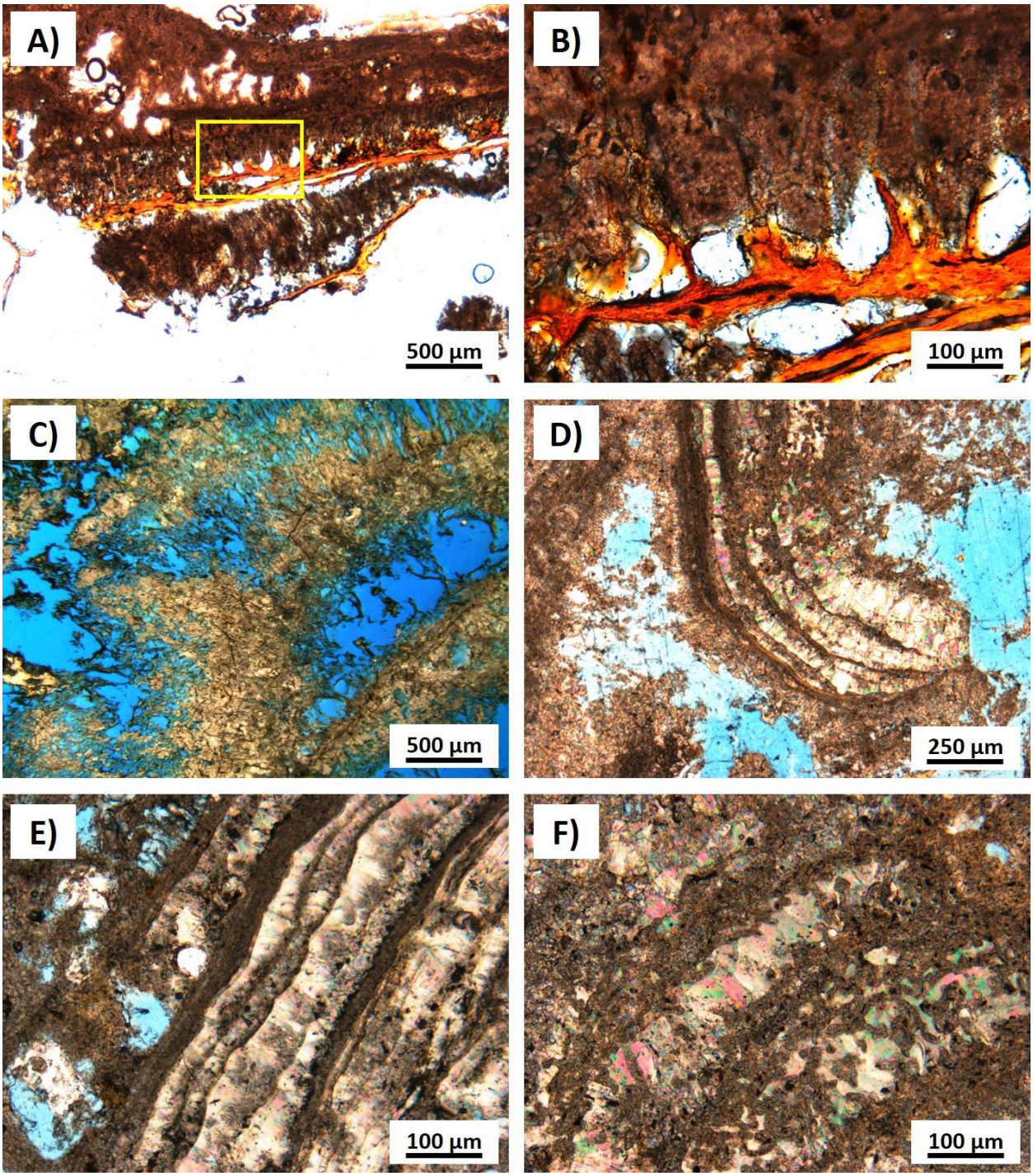

Figure 5: Microscopic components that make up micro- and macrofabrics of microbialites. A) Fibrous micrite (high-Mg calcite) associated with abundant organic matter (orange material) that is weakly calcified (Fabric 1). Location of (B) outlined by yellow box. B) Intimate association of organic matter with the fibrous micritic carbonates. C) More completely calcified fibrous micrite (Fabric 1). D) Clear fibrous and botryoidal aragonite that is discontinuous along trend, towards the bottom of the image (distinct botryoids). E) Clear fibrous and botryoidal aragonite that forms

more continuous laminae (coalesced botryoids). Note that botryoids can be superimposed, or separated by dense micritic laminae. F) Botryoids that are bored and partly to completely micritized. Progressive micritization could lead to destruction of laminae and create a more homogenous layer.

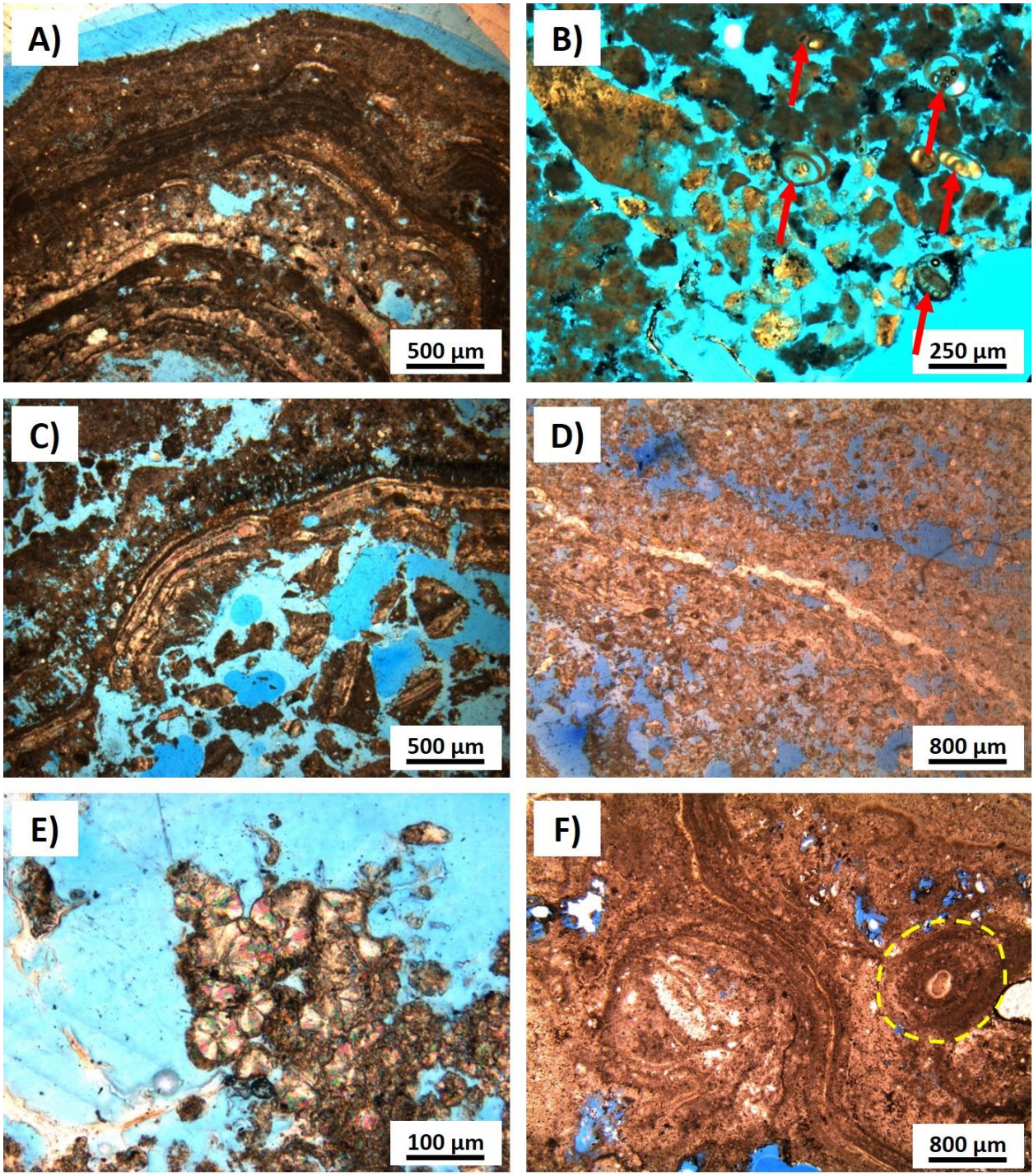

Figure 6: Microscopic components that make up micro- and macrofabrics of microbialites. A) Sub-mm wavy micritic laminae parallel to margins intimately associated with clear fibrous botryoids. B) Sedimentary particles are rare but can include forams (noted by red arrows) and mollusks (not shown in photomicrograph). C) Particles of angular, fitted fragments of components (e.g., a breccia). These types of features appear interlaminated with laminated micrite, botryoids laminations, and micritic carbonate. D) Homogeneous to clotted micrite, with common small

pores tens of μm in size, and no obvious internal structure is evident, although one clear, continuous botryoidal layer is evident.. E) Amalgamated and micritized spherules ~50 μm in diameter from near the edge of a microbialite. F) Individual spherule ~800 μm in diameter, from within a microbialite.

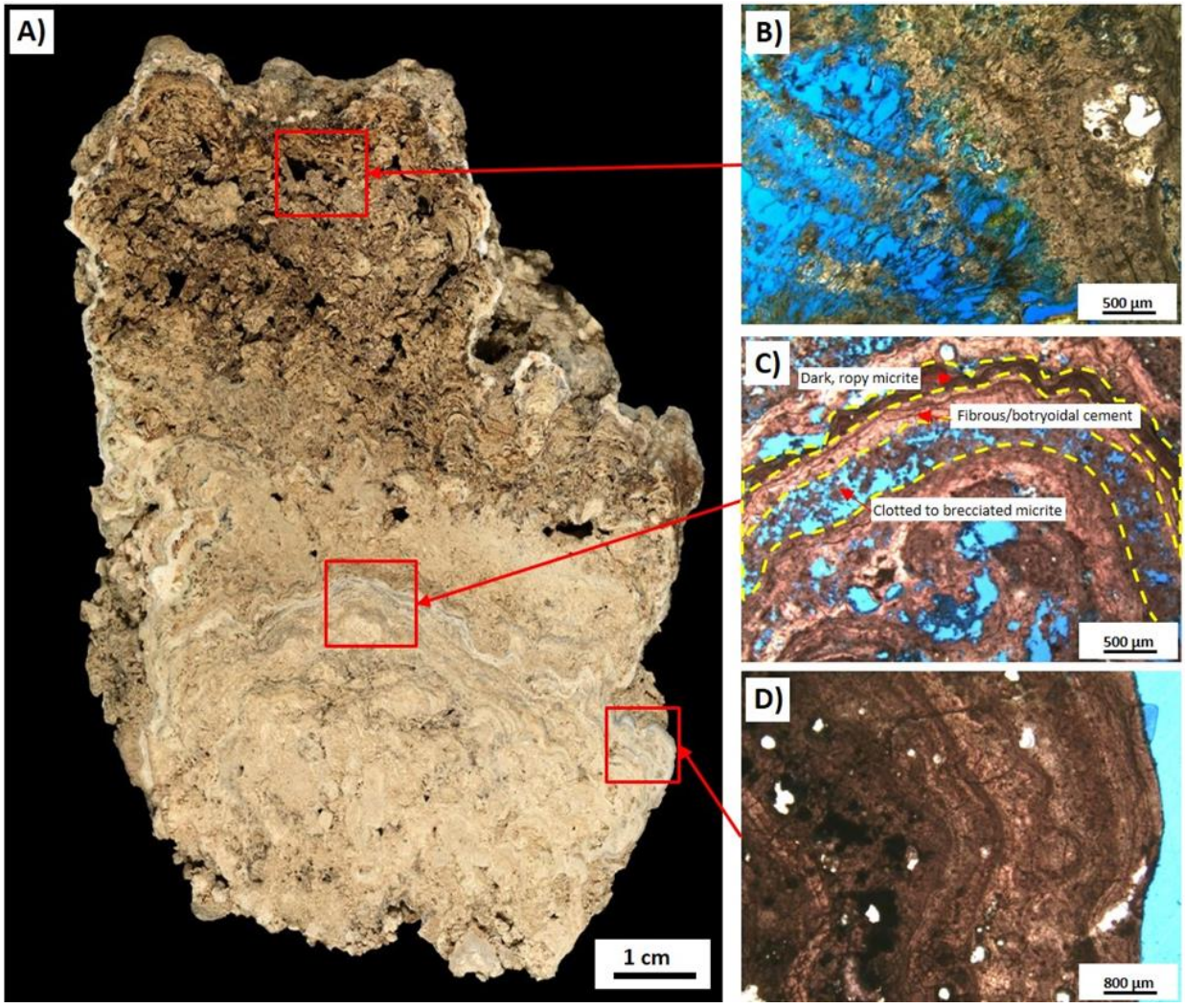

Figure 7: A) Photo of slab of representative microbialite. Locations of thin sections (shown in B-D) of three end-member microscopic fabrics are noted by red boxes. Although these end-members can be recognized as evident at some scales in many regions, a spectrum of intermediate fabrics can occur. B) Fabric 1: Organic matter and fibrous, ropy high-Mg calcite. The left side of this thin section shows a less calcified area, the region to the right illustrates a more completely calcified state. C) Fabric 2: Laminations made of alternations of dark micrite, fibrous to botryoidal aragonite cement, and clotted micrite with ubiquitous porosity. D) Fabric 3: Dense, tight laminations of dark micrite and clear(er) botryoidal aragonite cement. Laminations are roughly equal thicknesses (tens to hundreds of microns) and roughly parallel the present margin of the microbialite (e.g., at the right side of this image)

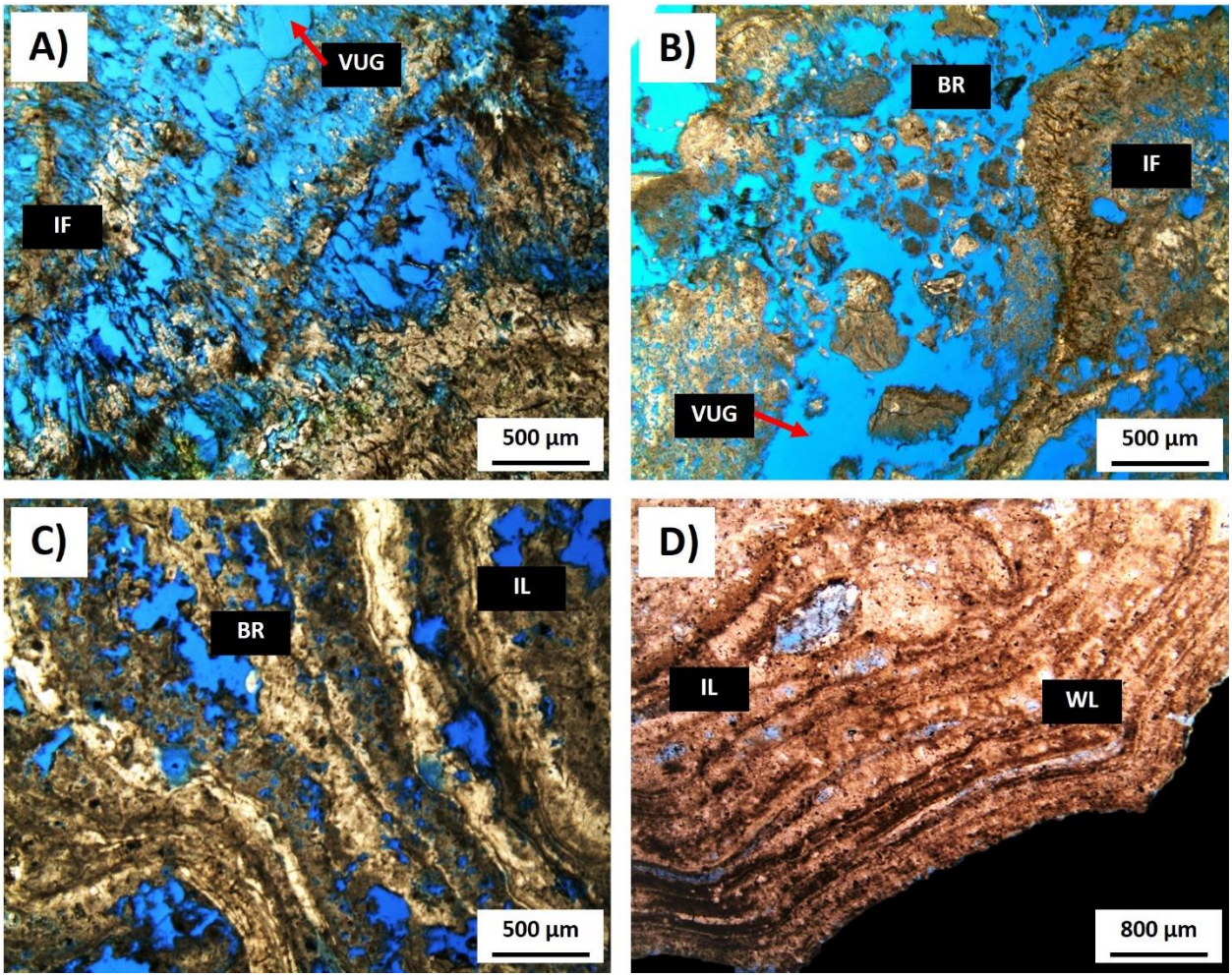

Figure 8: Petrographic classification of pores within Holocene microbialites. Pores are noted by blue epoxy. Although many pores likely represent open space within the framework, some likely are the result of desiccation of organic matter during thin section preparation. A) Fabric 1 = intra-fibrous (IF) and vuggy (VUG) pores (example noted by red arrow) and B) breccia (BR) pores associated with VUG pores (example noted by red arrow). Note that "vuggy porosity" as used here, follows Lucia (1995) to note pores larger than the component particles, rather than Choquette and Pray (1970), who used it to note solution-enlarged pores. C) Fabric 2 = inter-laminar (IL) and smaller pores related to clotted micrite. IL pores refer to elongate to sub-circular pores that are reflected in changes in thickness of laminations. D) Fabric 3 = IL and intra-laminar (WL) pores. Note WL pores refer to pores that are sheet-like and no or minimal disruption to surrounding laminae.

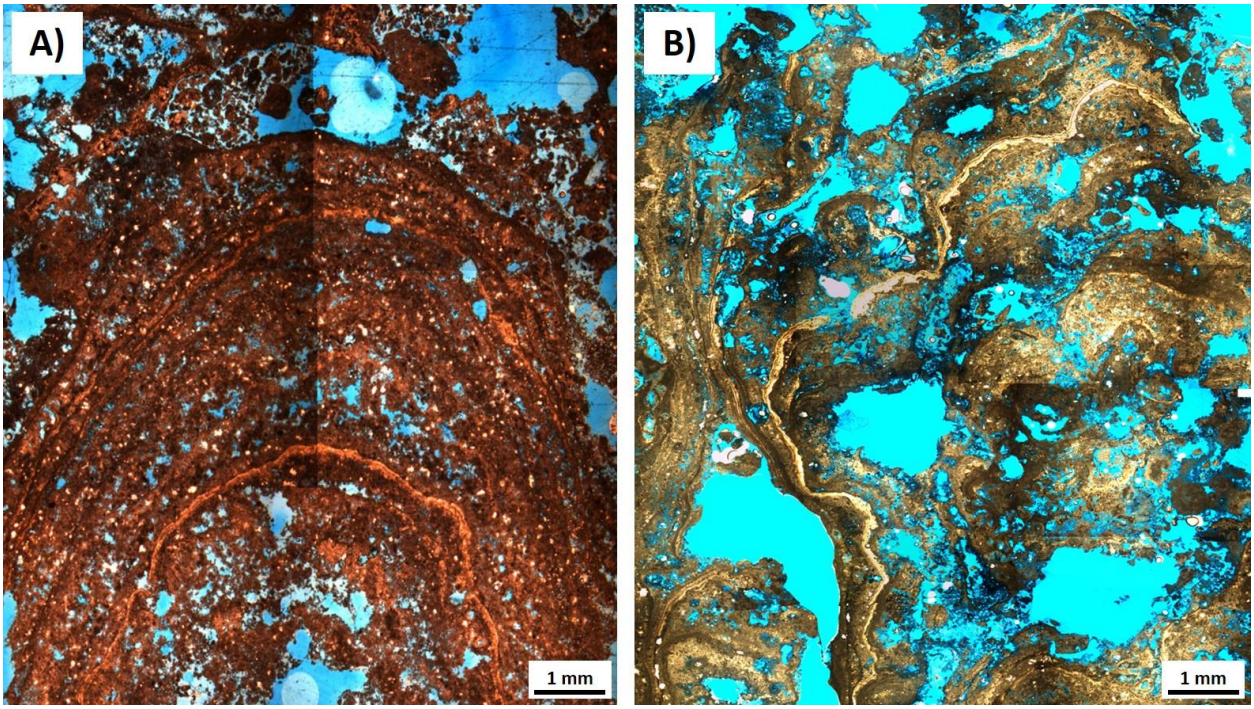

Figure 9: Thin-section photomicrographs illustrating microbialite macrofabrics. Blue notes pore space. A) Stromatolitic macrofabric. B) Thrombolitic macrofabric. Note that both macrofabrics include both Fabric 1 and Fabric 2, just in different abundance and configuration. These differences lead to distinct pore patterns.

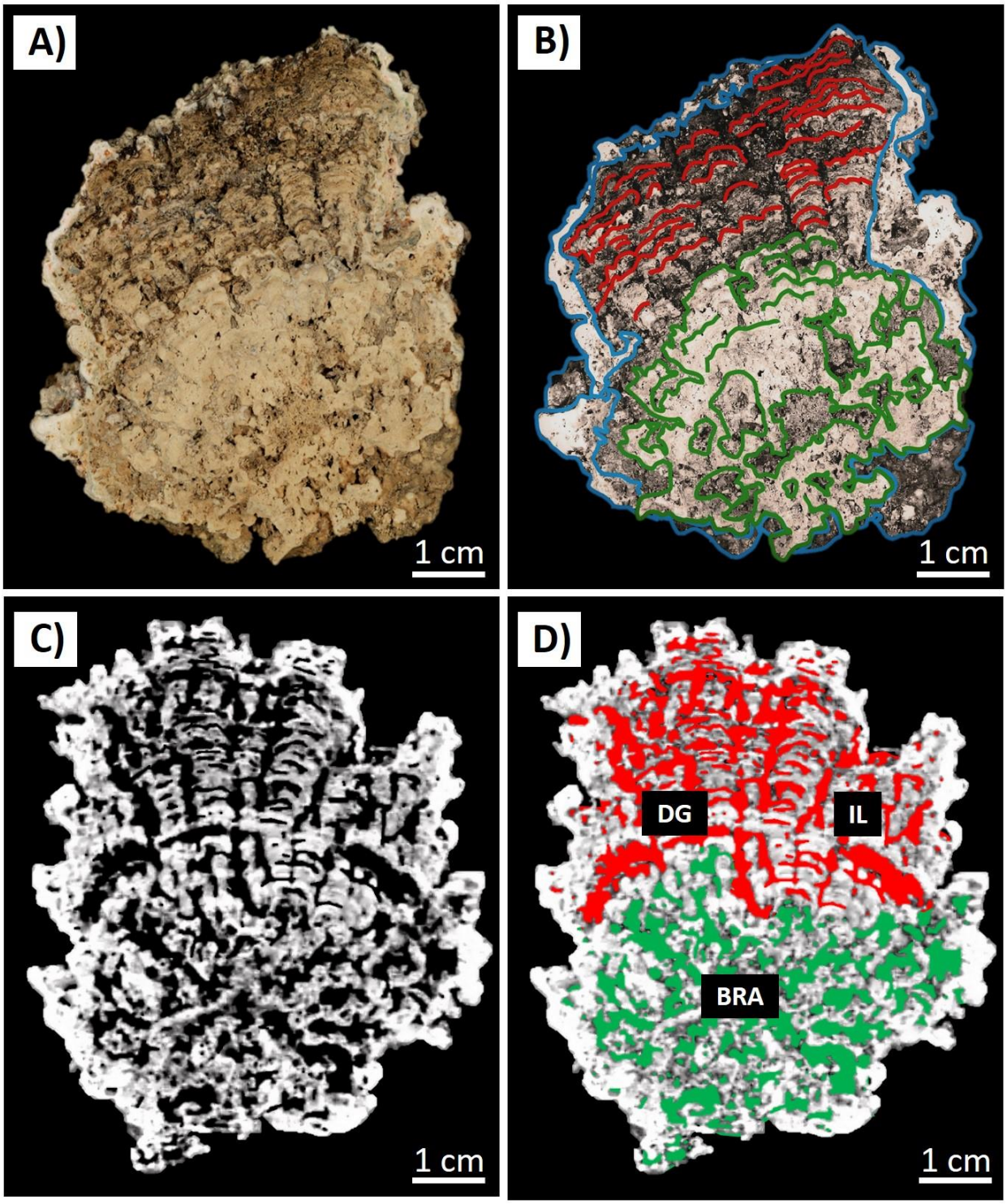

Figure 10: Representative Holocene calcareous microbialites (Bottom Type 5) illustrating macroscale depositional textures and associated pore attributes. A) Uninterpreted slabbed and polished photograph of microbialite. B) Macroscopic fabrics within the microbialite. Trace colors correspond to different general types of textures: Blue = bulbous outer coating of tight, micritic

laminations, Red = stromatolitic (laminated) fabric, and Green = thrombolitic (clotted) fabric. C) Representative 2D CT-scan horizon of an entire microbialite. D) Interpreted 2D CT-scan horizon illustrating the two distinct macroscopic-scale fabrics within microbialites. Red = traces of larger pores associated with the stromatolitic texture. Note both IL = inter-laminar porosity and DG = digitate pores. Green = traces of larger pores associated with thrombolitic to chaotic fabric and the branching (BRA) pores.

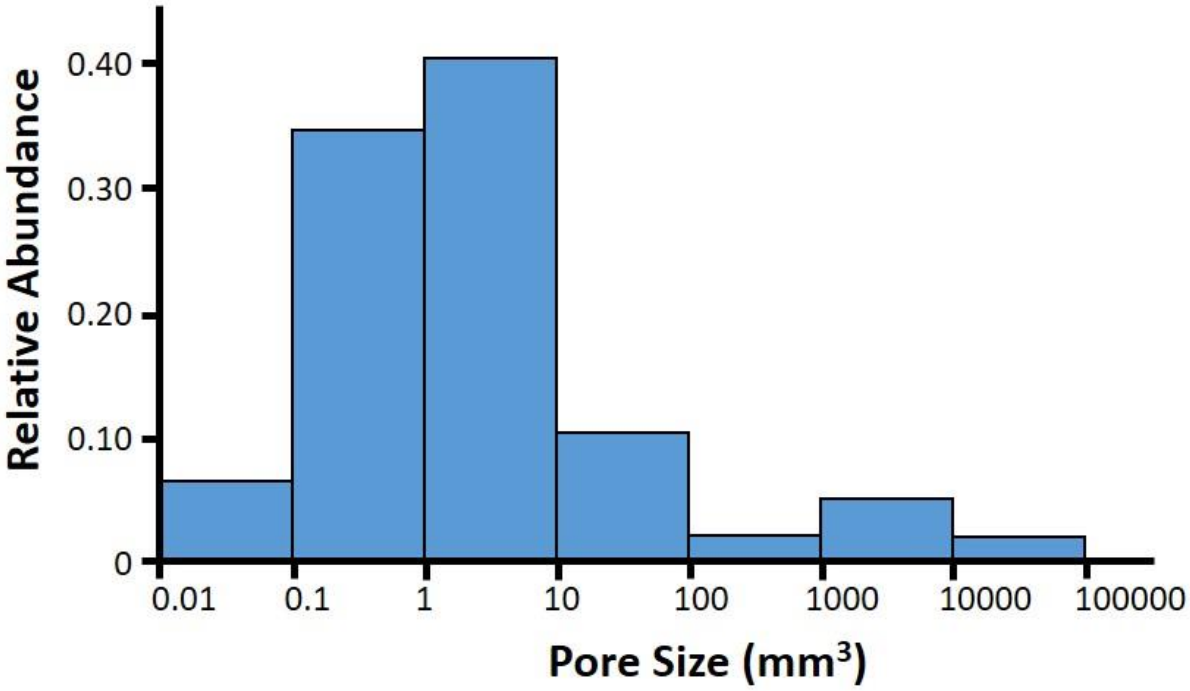

Figure 11: Avizo Fire 3D analysis of pore size distribution of a representative Holocene microbialite reveals considerable variability in pore sizes. Note that by this method, pores have a log-normal size frequency distribution, with a mode between 1-10 mm^3.

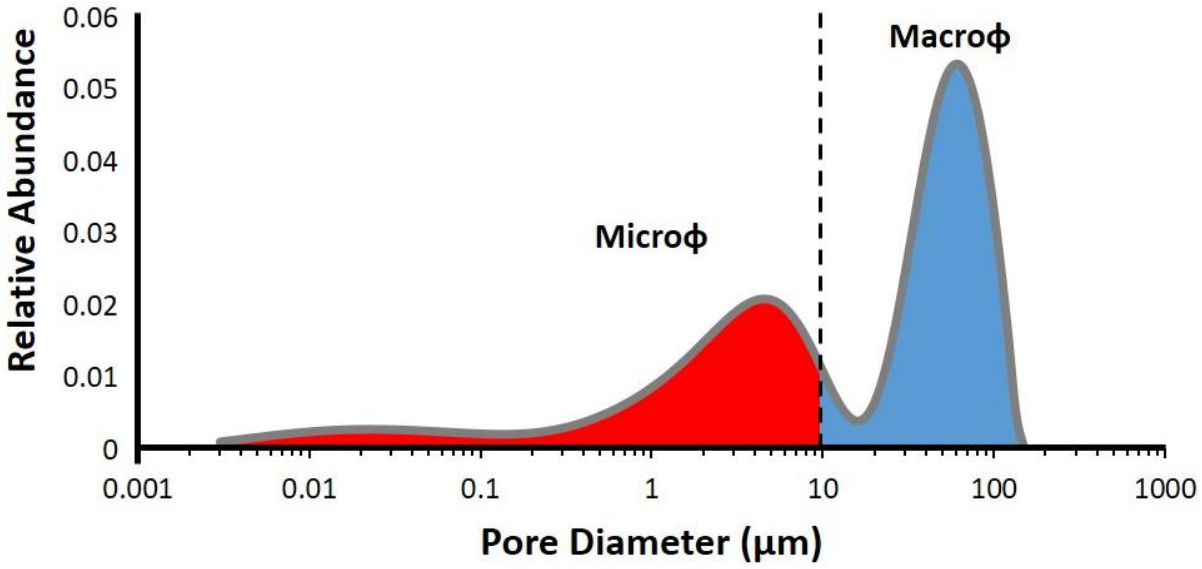

Figure 12: Representative NMR analysis from a Holocene microbialite core plug including all microfabrics illustrate a bi-modal distribution of pore sizes with macropores contributing to the greater part of the pore volume.

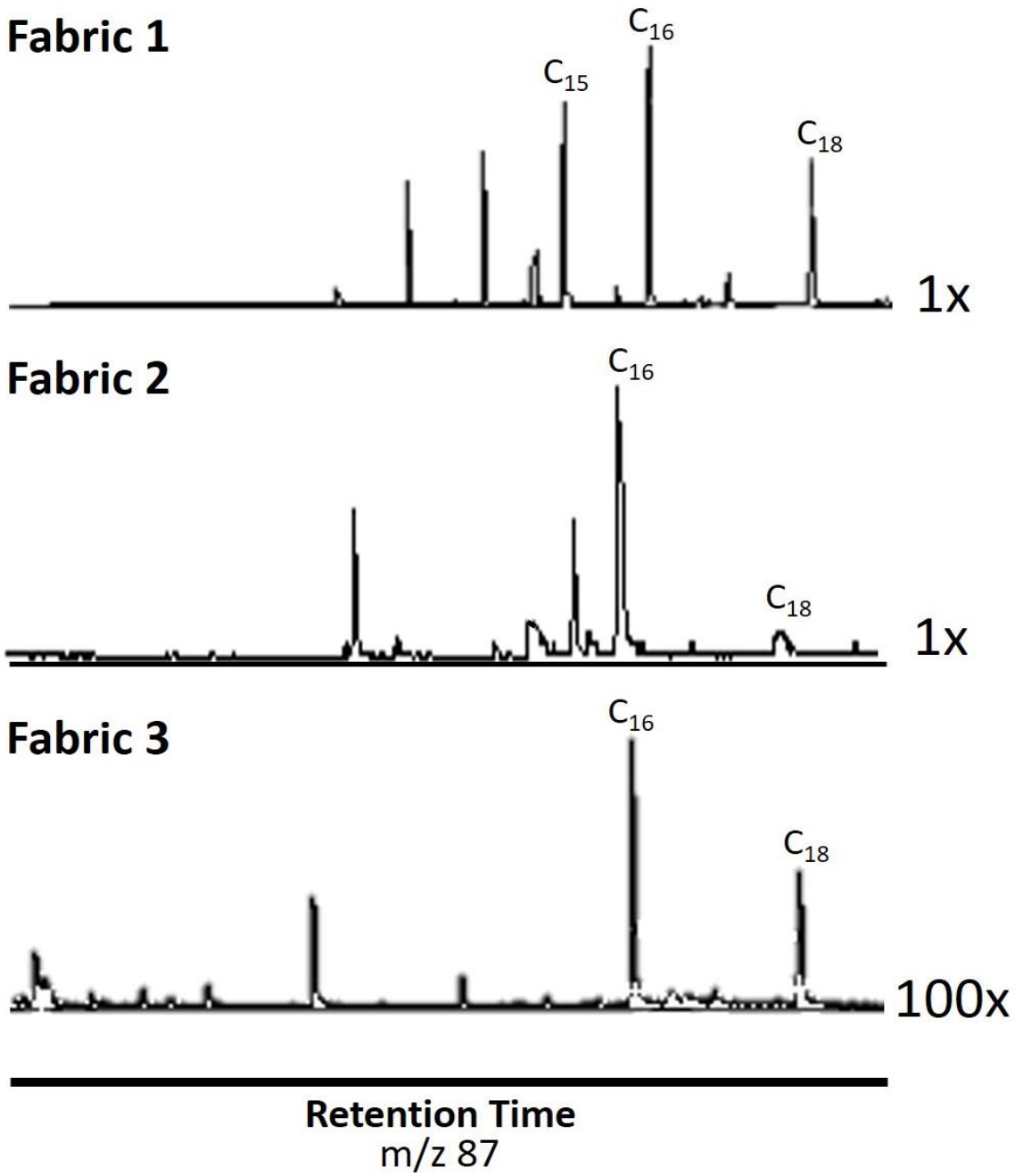

Figure 13: Representative GC/MS chromatograms of each microbialite end-member microfabric (Fabric 1, 2, and 3) documenting fragmentation patterns of abundant short chain fatty acids (C_{15}, C_{16}, C_{18}) indicative of fresh bacterial communities with no evidence for algae or higher plants or animals (m/z 87). 1x indicates the same concentration (Fabrics 1 and 2), whereas Fabric 3 is a hundredth as concentrated as Fabrics 1 and 2 indicated by the 100x. An equal amount of sample was analyzed between all fabrics, revealing Fabrics 1 and 2 contain a much higher abundance of extractable compounds compared to Fabric 3. In addition, Fabric 1 organic matter contains a broader suite of compounds (i.e., it is a more complex community of bacteria), it preserves more short chain fatty acids, or both compared to Fabrics 2 and 3.

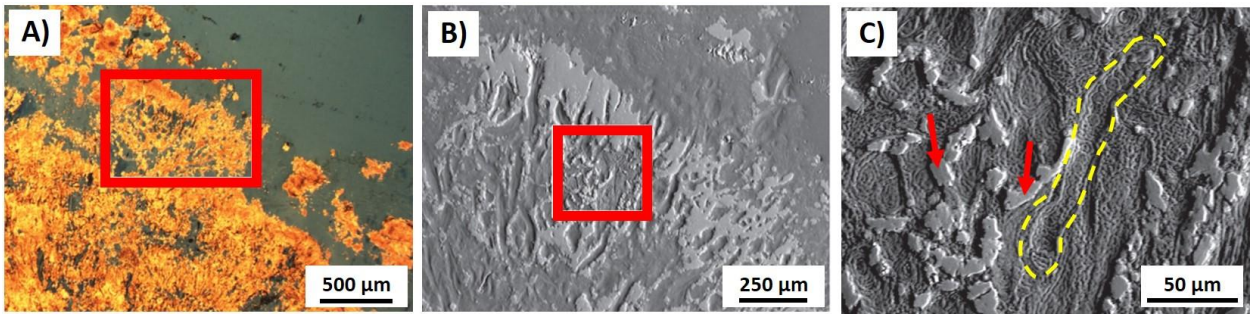

Figure 14: Organic matter growth habit within Holocene microbialites. A) Thin section photomicrograph of the outer edge of a microbialite. The fibrous micritic carbonates reflect and preserve a shrub-like morphology. Location of (B) noted by outlined red box. B) SEM image illustrating shrub-like carbonate morphology and its relation with filamentous microorganisms (inset darker grey areas). Location of (C) outlined by red box. C) Micritic carbonate (which makes up the fibers of the shrub, in part B; examples noted by red arrows) intimately associated with filamentous microorganisms (one is annotated by the yellow outline). Photomicrographs and SEM images courtesy of Christopher Omelon.

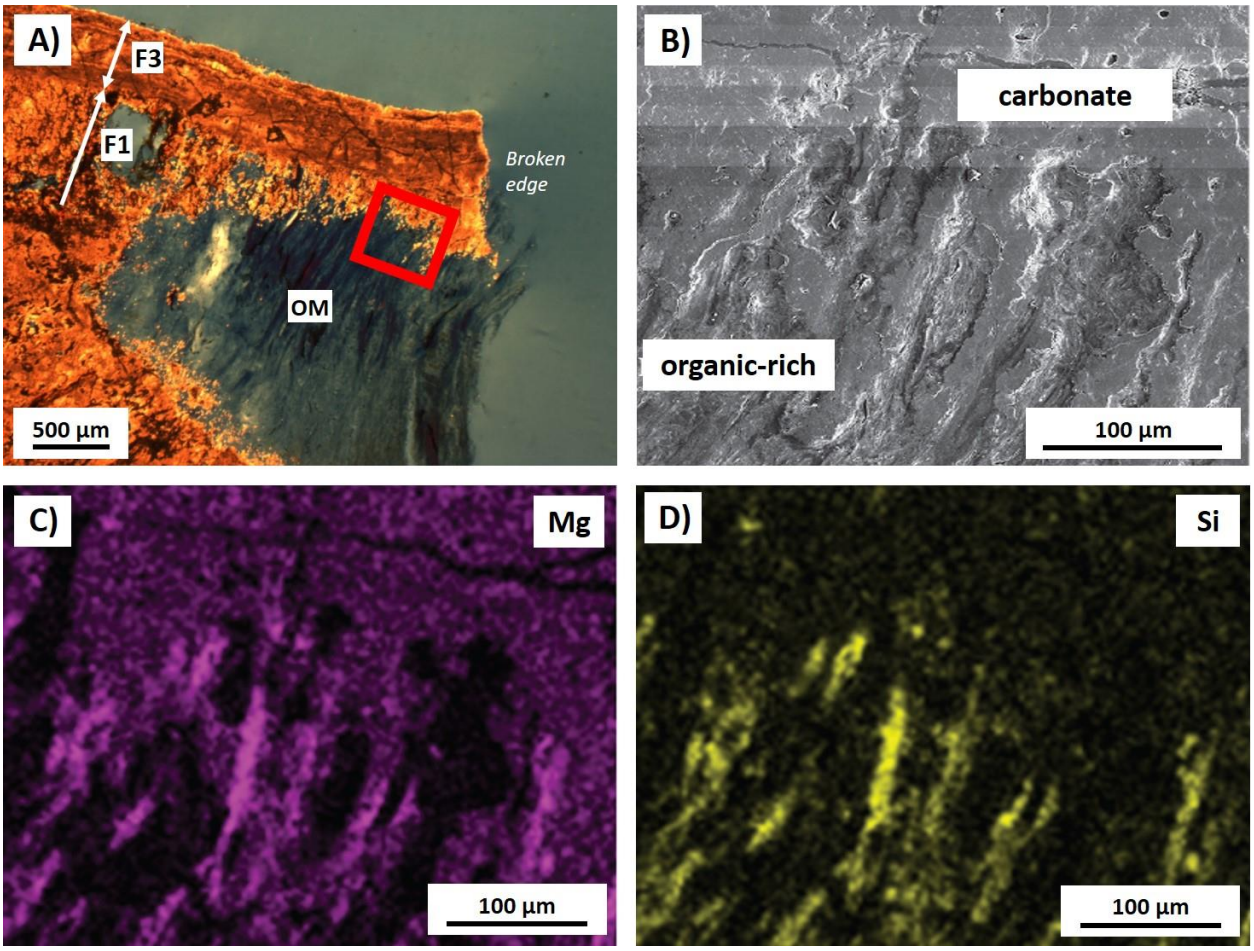

Figure 15: Petrographic, SEM, and energy dispersive spectroscopic (EDS) mapping of fabrics. A) Pore space within a microbialite bounded by tight, micritic laminations of carbonate above (F3), and fibrous and micritic carbonate below (F1). Location of (B) outlined in red box, and the right termination of the material is a broken edge. B) SEM micrograph showing carbonate (smooth) and organic matter (rough) textures. C-D) EDS mapping of area of inset in part A. (C) Purple = magnesium (Mg) and (D) Yellow = silica (Si). Note co-location of higher Mg and Si signals associated with the organic matter (D), suggesting the presence of Mg-silicates (probably in the form of amorphous gel). Images courtesy of Christopher Omelon.

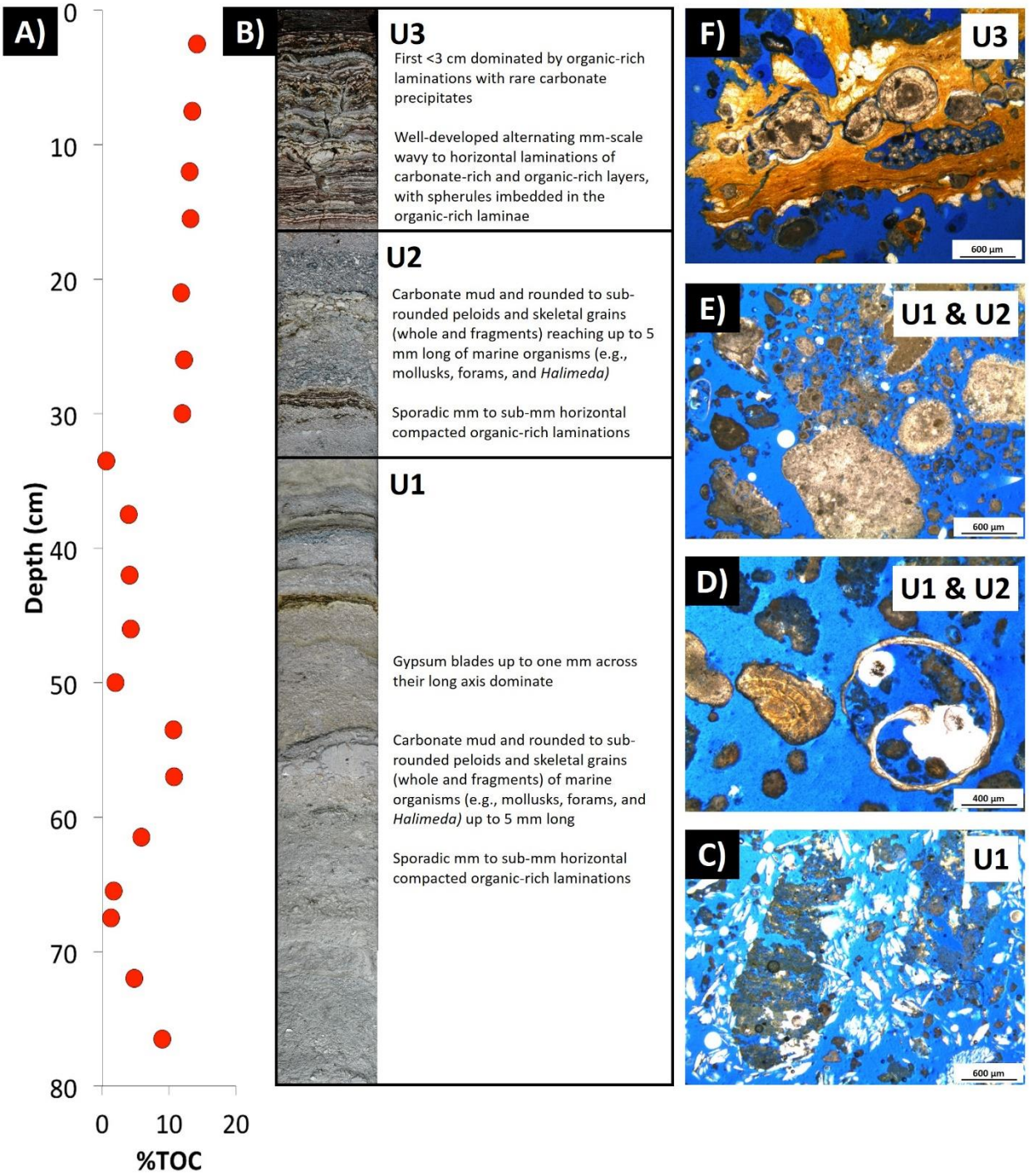

Figure 16: Windsor Point Salt Pond lake stratigraphy illustrated by a representative shallow (80 cm compacted and ~93 cm uncompacted) core taken from an area with Bottom Type 3 at the surface. A) TOC (%) plot for corresponding core in (B) with %TOC on the x-axis and depth on the y-axis. B) Core illustrates three units make it up (U1, U2, U3). Each includes distinct components, TOC abundance, and structures. C-F) Photomicrographs illustrate representative petrographic character of components corresponding to each unit. C) Evaporites common in U1

associated with carbonate mud and peloids. D) Skeletal grains (whole and fragments) of marine organisms (forams and mollusks in this photomicrograph), present sporadically in U2 and U1. E) Carbonate mud and rounded to sub-rounded peloids and occasional skeletal grains common in U1 and U2. F) Organic matter with embedded spherules, common in U3.

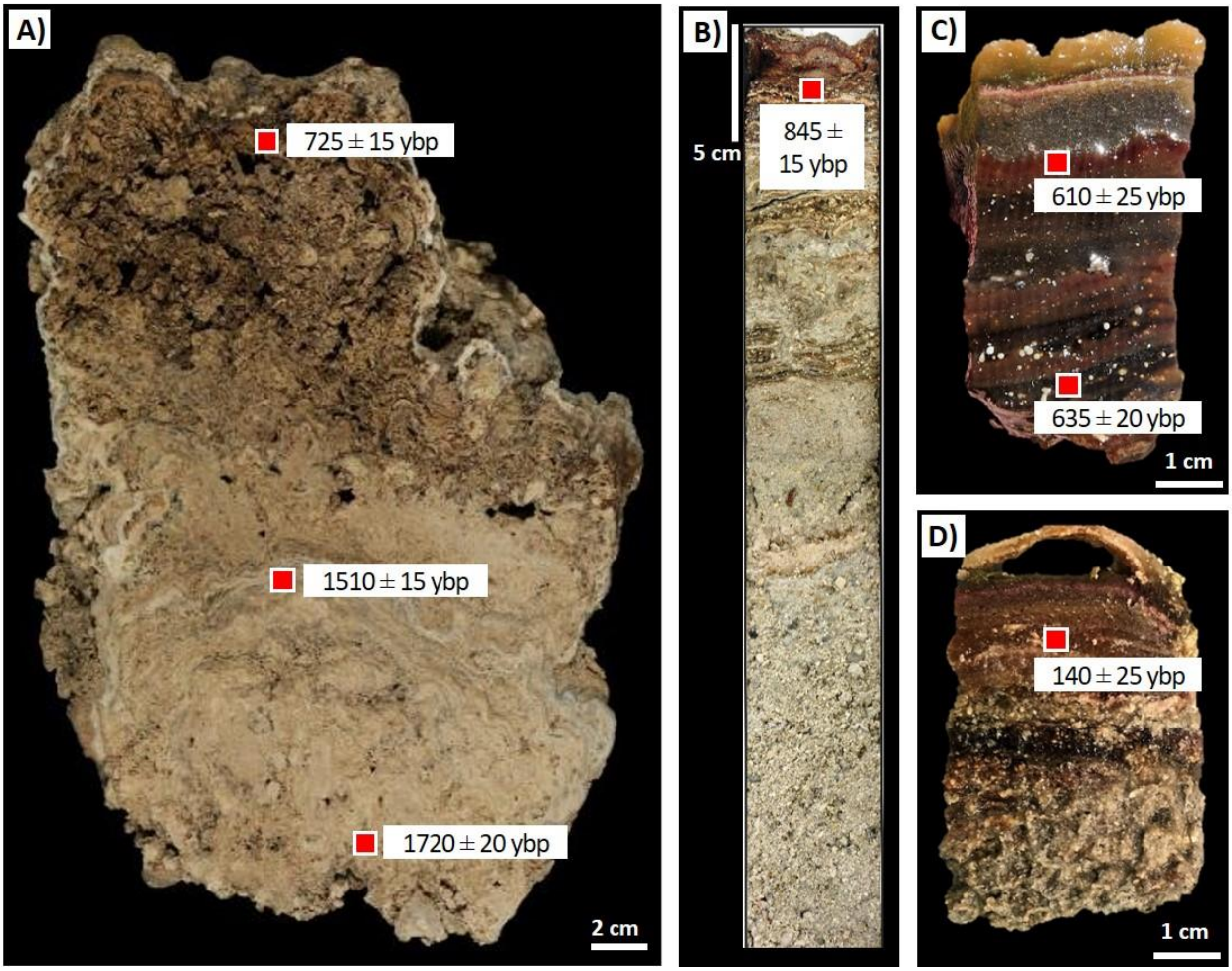

Figure 17: Sample locations of radiocarbon age dates of carbonate grains within representative microbialite and unlithified mats (noted by red boxes). A) Patterns from a calcareous microbialite. Growth stage of basal sample site dates 1720 ± 20 ybp. The middle sampling site dated at 1510 ± 15 ybp. Last growth stage 725 ± 15 ybp. Approximately 1000 years of ~25 cm of growth confirms rapid overall growth of 0.25 mm/yr, but with denser carbonate areas growing at a faster rate of 0.43 mm/yr. B) Carbonate sample from an unlithified mat ~3 cm below the sediment surface between microbialites revealed an age date of 845 ± 15 ybp. C) Two age dates from carbonate grains from this unlithified mat indicate carbonates are older downward (610 ± 25 ybp, down 3 cm to 635 ± 20 ybp). D) Unlithified mat collected at 60 m from the fringe of the lake at a water depth of ~30 cm had the youngest dated carbonates aged 140 ± 25 ybp.

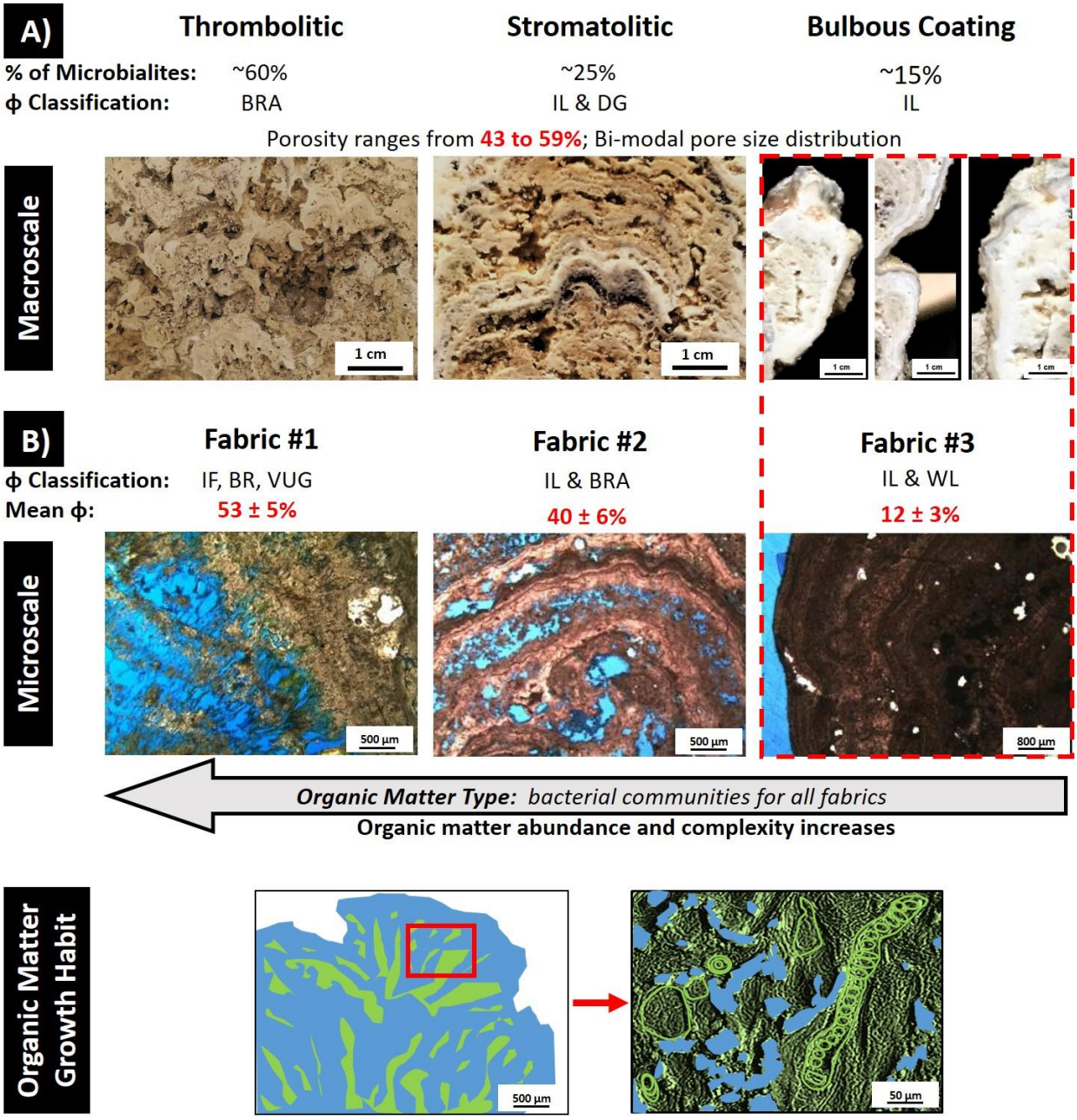

Figure 18: Summary of both macroscale and microscale fabrics. A) Macroscale fabrics including textures, pore attributes, and total porosity. B) Microscale end member fabrics including textures, pore types, total porosity, and source, abundance and growth habit of organic matter. Red outline indicates the bulbous outer coating is correlated to Fabric 3. See text for discussion.

Table

NMR Porosity Measurements		
Core Plug	Porosity (%)	Porosity Error (%)
1	59.70	0.20
2	64.80	0.20
3	55.40	0.20
4	59.00	0.10
5	58.60	0.20
6	50.63	0.10
7	64.30	0.10
8	69.40	0.10
9	48.05	0.09
10	58.30	0.10
11	60.20	0.10
Mean Porosity		**58.94%**
Standard Deviation		**5.84%**

Table 1: NMR measurements of 11 core plugs from within microbialites. Each plug contains a mix of two or more fabrics. These results illustrate high porosity associated with these microbialites at the core plug scale (mean porosity = 59 ± 6%).

Appendix I – NMR Pore Size Distribution Graphs

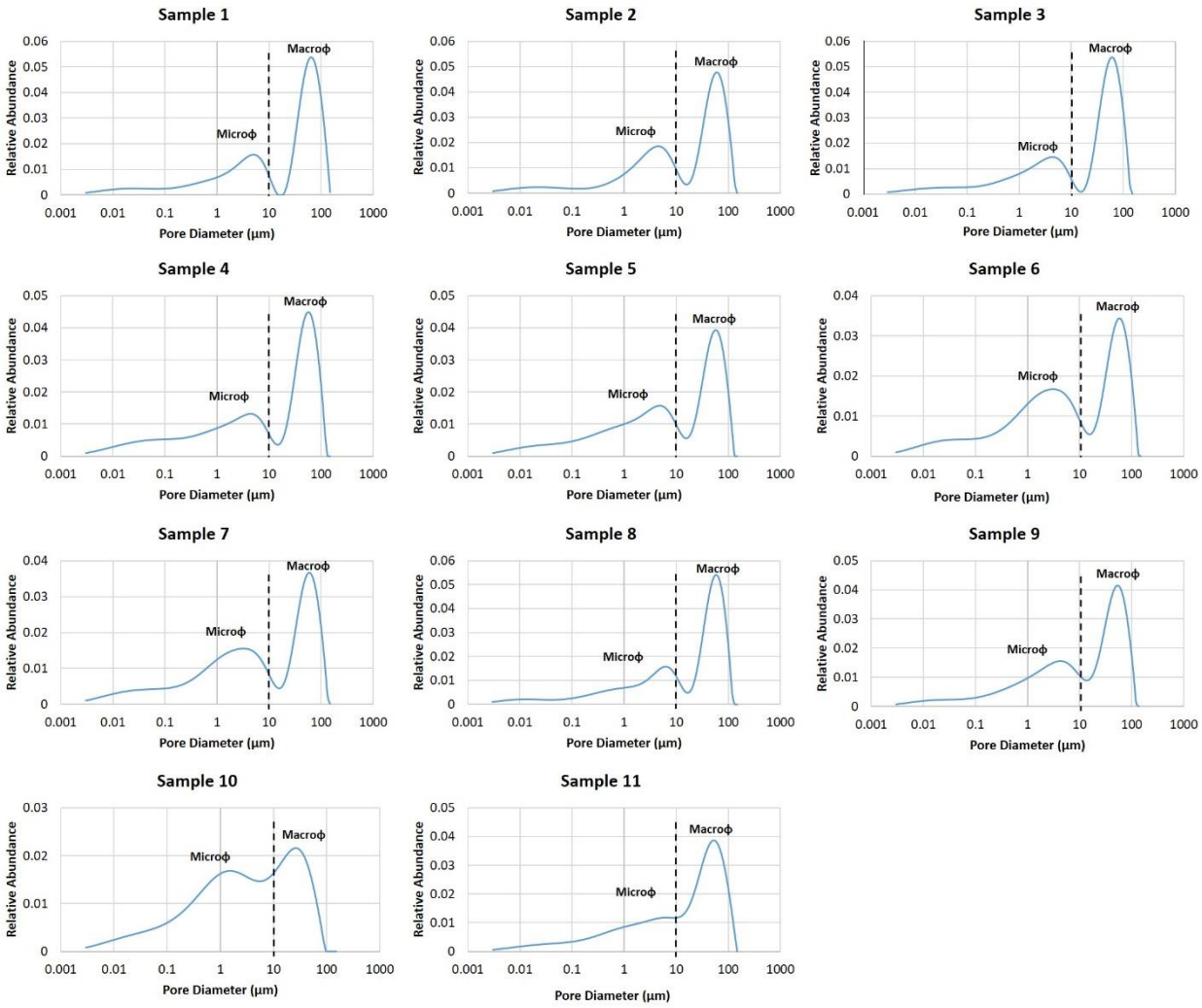

NMR analyses of all eleven Holocene microbialite core plugs including all microfabrics illustrating a bi-modal distribution of pore sizes with macropores contributing to most of the pore volume.

Appendix II – GC/MS Chromatograms

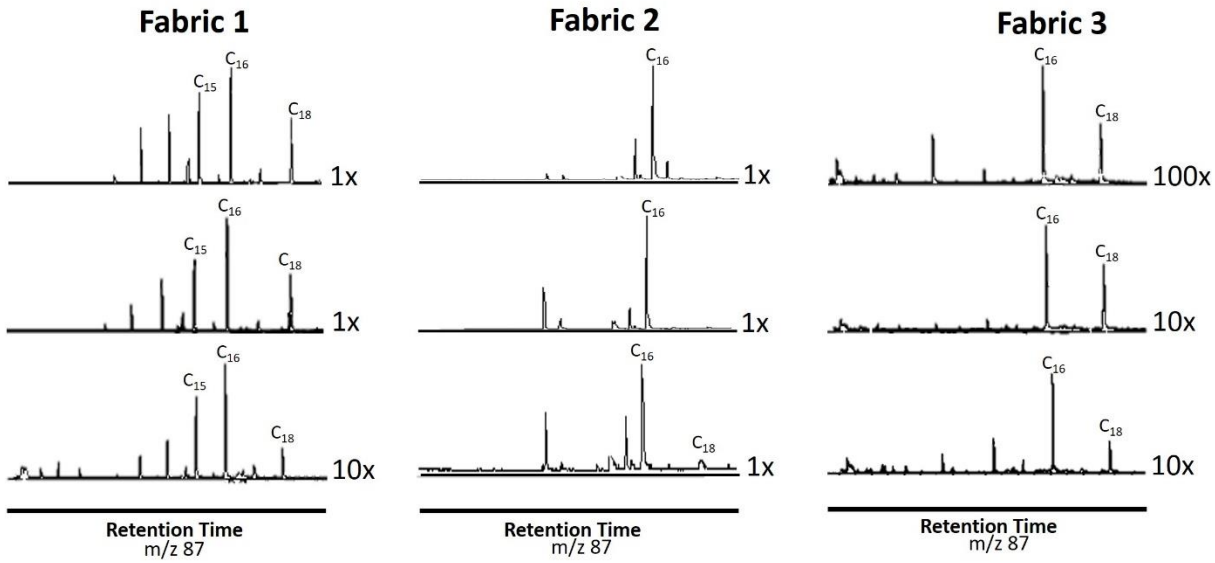

GC/MS chromatograms of all samples including all end-member microfabrics displaying fragmentation patterns of abundant short chain fatty acids (C_{15}, C_{16}, C_{18}) indicating organic matter is dominantly composed of bacterial communities with no evidence for algae or higher plants or animals (m/z 87) for all microfabrics. 1x indicates the same concentration, whereas samples listed at 10x and 100x are a tenth and one hundredth as concentrated, respectively. Equal amounts of samples were analyzed, therefore, Fabrics 1 and 2 contain a greater amount of extractable organic matter compared to Fabric 3. Also, Fabric 1 organic matter contains a broader suite of compounds (i.e., it is a more complex community of bacteria), it preserves more short chain fatty acids, or both compared to Fabrics 2 and 3.

Appendix III – Radiocarbon Age Dating Hydrolysis Method

To begin the process, ~50 mg of each sample was crushed, ca. ~10 mg were acidified and the evolved CO_2 was graphitized (Gagnon and Jones, 1993). The remaining ~40 mg of powdered carbonate were saved for the two remaining blanks resulting in each successive blank giving increasingly higher backgrounds due to adsorption of atmospheric CO_2 onto the carbonate (Gagnon and Jones, 1993). About 15-20 mg of each blank sample were placed in a pre-cleaned beaker and acidified for 1-3 min with 10% organic-free HCl (Froelich 1990). The carbonate samples, rinsed thoroughly with double-distilled water (Froelich 1990) to remove the acid, were placed in a 50°C oven until dry. A pre-cleaned agate mortar and pestle crushed the sample to a fine powder (10-15 mg) that was transferred to a glass reaction vessel and hydrolyzed (Gagnon and Jones, 1993). Four ml of 85% phosphoric acid was added to the side arm of the reaction vessel, and a glass-plug vacuum valve was connected to the vessel (Gagnon and Jones 1993). Once vacuum was achieved, the valve was closed, the vessel removed from the vacuum line and the acid warmed to ambient temperature (Gagnon and Jones 1993). The vessel was tilted manually to allow the acid to flow from the side arm until it made contact with the carbonate sample. Acid was added slowly and then the acid/sample mixture was heated to near boiling with a Bunsen burner every 30 min until no reaction was observed (Gagnon and Jones 1993). Once the ~2 hr reaction was completed, the vessel was re-attached to the vacuum line, a dry ice/isopropanol slush trap was attached to the lower finger of the reaction vessel, a second dry ice/isopropanol slush trap was attached to the vacuum line, the reaction vessel was opened and the gas was transferred cryogenically for 3-4 min to a region of known volume (Gagnon and Jones 1993). The CO_2 was expanded in the known-volume region, warmed to ambient temperature, measured a pressure transducer and transferred directly to the graphite reactor (Gagnon and Jones 1993). The graphitization procedure is based on the conventional technique of iron-catalyzed reduction of CO2 to graphite in the presence of hydrogen at 630 °C and was conducted as described by Bird et al. (1999) (Gagnon and Jones 1993). The "graphite" derived from a sample is compressed into a small cavity in an aluminum "target" which acts as a cathode in the ion source (Gagnon and Jones, 1993). The surface of the graphite is sputtered with heated, ionized cesium and the ions produced are extracted and accelerated in the AMS system (Gagnon and Jones, 1993). After acceleration and removal of electrons, the emerging positive ions are magnetically separated by mass and the ^{12}C and ^{13}C ions are measured in Faraday Cups where a ratio of their currents is recorded (Gagnon and Jones, 1993). Simultaneously the ^{14}C ions are recorded in a gas ionization detector, so that ratios of ^{14}C to ^{13}C and ^{12}C may be recorded and these raw signals were ultimately converted to a radiocarbon age (Gagnon and Jones, 1993).

Appendix IV – Radiocarbon Age Dates

Microbialite Radiocarbon Dates:

Date Reported	Submitter Identification	Type	Process	Accession #	F Modern	Fm Err	δ13C Corr	Age	Age Err	δ13C Source
1/22/2016	BA-1 (top)	Sediment Inorganic Carbon	(HY) Hydrolysis	OS-123540	0.9139	0.0018	*	725	15	Not Measured
1/22/2016	BA-2 (middle)	Sediment Inorganic Carbon	(HY) Hydrolysis	OS-123541	0.8289	0.0018	*	1,510	15	Not Measured
1/22/2016	BA-3 (bottom)	Sediment Inorganic Carbon	(HY) Hydrolysis	OS-123542	0.8073	0.0020	*	1,720	20	Not Measured
1/22/2016	SB-1 (top)	Sediment Inorganic Carbon	(HY) Hydrolysis	OS-123543	0.8148	0.0032	*	750	30	Not Measured
1/22/2016	SB-2 (middle)	Sediment Inorganic Carbon	(HY) Hydrolysis	OS-123544	0.8072	0.0018	*	1,720	20	Not Measured
1/22/2016	SB-3 (bottom)	Sediment Inorganic Carbon	(HY) Hydrolysis	OS-123545	0.8090	0.0018	*	1,700	20	Not Measured

Microbial Mats Radiocarbon Dates:

Date Reported	Submitter Identification	Type	Process	Accession #	F Modern	Fm Err	δ13C Corr	Age	Age Err	δ13C Source	Δ14C
1/26/2017	HH3-6T (mat)	Sediment Inorganic Carbon	(HY) Hydrolysis	OS-130705	0.9270	0.0028	*	610	25	Not Measured	-80.39
1/26/2017	HH3-6B (mat)	Sediment Inorganic Carbon	(HY) Hydrolysis	OS-130706	0.9237	0.0020	*	635	20	Not Measured	-83.61
1/26/2017	HH-CT (core)	Sediment Inorganic Carbon	(HY) Hydrolysis	OS-130707	0.9003	0.0018	*	845	15	Not Measured	-106.88
1/26/2017	HH2-3 (mat)	Sediment Inorganic Carbon	(HY) Hydrolysis	OS-130708	0.9830	0.0033	*	140	25	Not Measured	-24.81

** The asterisks indicate that the radiocarbon result was corrected for isotopic fractionation using unreported d13C values measured on the accelerator.*

Results from two microbialites (upper table) and three microbial mats (lower table).